Topological color codes and two-body quantum lattice Hamiltonians

2010 New J. Phys. 12 025018

(http://iopscience.iop.org/1367-2630/12/2/025018)

New Journal of Physics
The open-access journal for physics

Topological color codes and two-body quantum lattice Hamiltonians

M Kargarian[1], H Bombin[2] and M A Martin-Delgado[3]

[1] Physics Department, Sharif University of Technology, Tehran 11155-9161, Iran

[2] Department of Physics, Massachusetts Institute of Technology, Cambridge, MA 02139, USA

[3] Departamento de Física Teórica I, Universidad Complutense, 28040 Madrid, Spain

E-mail: mardel@miranda.fis.ucm.es

New Journal of Physics **12** (2010) 025018 (40pp)
Received 21 June 2009
Published 26 February 2010
Online at http://www.njp.org/
doi:10.1088/1367-2630/12/2/025018

Abstract. Topological color codes are among the stabilizer codes with remarkable properties from the quantum information perspective. In this paper, we construct a lattice, the so-called ruby lattice, with coordination number 4 governed by a two-body Hamiltonian. In a particular regime of coupling constants, in a strong coupling limit, degenerate perturbation theory implies that the low-energy spectrum of the model can be described by a many-body effective Hamiltonian, which encodes the color code as its ground state subspace. Ground state subspace corresponds to a vortex-free sector. The gauge symmetry $\mathbf{Z}_2 \times \mathbf{Z}_2$ of the color code could already be realized by identifying three distinct plaquette operators on the ruby lattice. All plaquette operators commute with each other and with the Hamiltonian being integrals of motion. Plaquettes are extended to closed strings or string-net structures. Non-contractible closed strings winding the space commute with Hamiltonian but not always with each other. This gives rise to exact topological degeneracy of the model. A connection to 2-colexes can be established via the coloring of the strings. We discuss it at the non-perturbative level. The particular structure of the two-body Hamiltonian provides a fruitful interpretation in terms of mapping onto bosons coupled to effective spins. We show that high-energy excitations of the model have fermionic statistics. They form three families of high-energy excitations each of one color. Furthermore, we show that they belong to a particular family of topological charges. The emergence of invisible charges is related to the string-net structure of the model.

The emerging fermions are coupled to nontrivial gauge fields. We show that for particular 2-colexes, the fermions can see the background fluxes in the ground state. Also, we use the Jordan–Wigner transformation in order to test the integrability of the model via introducing Majorana fermions. The four-valent structure of the lattice prevents the fermionized Hamiltonian from being reduced to a quadratic form owing to interacting gauge fields. We also propose another construction for the two-body Hamiltonian based on the connection between color codes and cluster states. The corresponding two-body Hamiltonian encodes a cluster state defined on a bipartite lattice as its low-energy spectrum, and subsequent selective measurements give rise to the color code model. We discuss this latter approach along with the construction based on the ruby lattice.

Contents

1. Introduction

Topological color codes (TCCs) are a whole class of models that provide an instance of an interdisciplinary subject between quantum information and the physics of quantum many-body systems.

TCCs were introduced [1] as a class of topological quantum codes that allow direct implementation of the Clifford group of quantum gates suitable for entanglement distillation, teleportation and fault-tolerant quantum computation. They are defined on certain types of two-dimensional (2D) spatial lattices. They were extended to 3D lattices [2] in order to achieve universal quantum computation with TCCs. This proposal of topological quantum computation relies solely on the topological properties of the ground state sector of certain lattice Hamiltonians, without resorting to braiding of quasi-particle excitations. In addition to

these applications in quantum information, TCCs also have a natural application in strongly correlated systems of condensed matter with topological orders (TOs). In [3], it was found that TCCs can be extended to arbitrary dimensions, giving rise to TOs in any dimension, not just 2D. This is accomplished through the notion of D-colexes, which are a class of lattices with certain properties where quantum lattice Hamiltonians are defined. This corresponds to a new class of exact models in $D = 3$ and higher dimensions that exhibit new mechanisms for TO: (i) brane-net condensation; (ii) existence of branyons; (iii) higher ground-state degeneracy than other codes; (iv) different topological phases for $D \geqslant 4$, etc. In what follows, we shall focus only on 2D lattices.

Physically, TCCs are exotic quantum states of matter with novel properties. They are useful for implementing topological quantum computation, but they have also an intrinsic interest of their own. Then, a natural question arises as to how to implement experimentally these new quantum systems by means of light, atoms or some other means. This is a challenge, since TCCs are formulated in terms of Hamiltonians with many-body terms, the simplest having six-body interactions in a hexagonal lattice. But the most common interactions in nature are typically two-body interactions.

There are several approaches trying to solve this challenge, depending on the type of scenario we envision to be in practice and the practical rules we are supposed to be allowed to have at our disposal.

Let us start first with what we may call a 'quantum control scenario'. By this we simply mean that we are able to perform very controllable quantum operations on our system that we have prepared artificially. In particular, we suppose that we can perform quantum measurements on the qubits and have ancilla qubits at will. Under these circumstances, we can resort to cluster states [4] and measurement-based quantum computation [5, 6]. This is because TCCs can be described by a certain cluster state construction [7] within this scenario. Then, it is possible to use a technique to obtain graph states as ground states of two-body qubit Hamiltonians [8, 9]. We show this construction in the appendix. However, this scenario is experimentally very demanding and it is left for the future when it will be achieved completely. Therefore, it is convenient to seek other alternatives.

Thus, let us move onto a 'condensed matter scenario'. The terminology is intended just to be illustrative, rather than precise. In fact, the scenario goes beyond condensed matter and may well be a quantum simulation of our system by means of engineering a set of photons, atoms or the like. The important difference now is that external measurements on the system, or ancilla qubits, are not allowed in order to obtain the desired Hamiltonian for the TCCs. We want to remain in a framework based on Hamiltonians with solely two-body interactions [10].

We have introduced a new quantum two-body Hamiltonian on a 2D lattice with results that follow the two-fold motivation concerning topics in quantum information and quantum many-body systems:

(i) to achieve scalable quantum computation [11]–[13] and
(ii) to perform quantum simulations with light, atoms and similar available means [14]–[23].

This is so because, on the one hand, the Hamiltonian system that we introduce is able to reproduce the quantum computational properties of the TCCs [1]–[3] at a non-perturbative level as explained in section 4. This is an important step towards obtaining topological protection against decoherence in the quest for scalability. On the other hand, the fact that the interactions in the Hamiltonian appear as two-body spin (or qubit) terms makes it more suitable for its

realization by means of a quantum simulation based on available physical proposal with light and atoms.

In the framework of strongly correlated systems in quantum many-body systems, one of the several reasons for being interested in the experimental implementation of this Hamiltonian system is because it exhibits exotic quantum phases of matter known as TOs, some of its distinctive features being the existence of anyons [24]–[26]. In our everyday 3D world, we only deal with fermions and bosons. Thus, exchanging a pair of particles twice is a topologically trivial operation. In 2D, this is no longer true, and particles with other statistics are possible: anyons. When the difference is just a phase, the anyons are called Abelian. Anyons are a signature of TO [27, 28], and there are others as well:

- there is an energy gap between the ground state and the excitations;
- topological degeneracy of the ground state subspace (GS);
- this degeneracy cannot be lifted by local perturbations;
- localized quasi-particles as excited states: anyons;
- edge states; etc.

These features reflect the topological nature of the system. In addition, a signature of the TO is the dependence of that degeneracy on topological invariants of the lattice where the system is defined, such as Betti numbers [3].

But where do we find TOs? These quantum phases of matter are difficult to find. If we are lucky, we may find them on existing physical systems such as the quantum Hall effect. But we can also engineer suitable quantum Hamiltonian models, e.g. using polar molecules on optical lattices [14, 15, 20], or by some other means. There are methods for demonstrating TO without resorting to interferometric techniques [29].

In this paper, we present new results concerning the realization of two-body Hamiltonians using cluster states techniques on the one hand, and without measurement-based computations on the other hand. In the latter case, we present a detailed study of the set of integrals of motion (IOM) in a two-body Hamiltonian, fermionic mappings of the original spin Hamiltonian that give information about the physics of the system and that complement previous results using bosonic mapping techniques [10].

The paper is organized as follows: in section 2, we present color codes as instances of topological stabilizer codes with Hamiltonians based on many-body interacting terms and we then introduce the quantum Hamiltonian model based solely on two-body interactions between spin-$\frac{1}{2}$ particles. The lattice is 2D and has coordination number 4, instead of the usual 3 for the Kitaev model. It is shown in figure 3 and is called the ruby lattice. In section 3, we describe the structure of the set of exact IOM of the two-body model. We give a set of diagrammatic local rules that are the building blocks to construct arbitrary IOMs. These include colored strings and string-nets constants of motion, which is a distinctive feature with respect to Kitaev's model. In section 4, we establish a connection between the original TCC and the new two-body color model. This is done firstly at a non-perturbative level using the colored string IOM that are related to the corresponding strings in the TCC. Then, using degenerate perturbation theory (PT) in the Green function formalism, it is possible to describe a gapped phase of the two-body color model that corresponds precisely to the TCC. In section 5, we introduce a mapping from the original spin-$\frac{1}{2}$ degrees of freedom onto bosonic degrees of freedom in the form of hard-core bosons, that also carry a pseudospin. This provides an alternative way to perform PT

and obtain the gapped phase corresponding to the TCC. It also provides a nice description of low energy properties of the two-body model and its quasi-particles. In section 6, we introduce another mapping based on spinless fermions, that is helpful to understand the structure of the two-body Hamiltonian and the presence of interacting terms that are related to the existence of string-nets constants of motion. Section 7 is devoted to conclusions and future prospects. The appendix describes how to obtain two-body Hamiltonians for TCCs based on cluster states and measurements using ancilla qubits.

2. Quantum lattice Hamiltonian with two-body interactions

2.1. Color codes as topological stabilizers

Some of the simplest quantum Hamiltonian models with TO can be obtained from a formalism based on the local stabilizer codes borrowed from quantum error correction [30] in quantum information [31, 32]. These are spin-$\frac{1}{2}$ local models of the form

$$H = -\sum_i S_i, \quad S_i \in \mathbf{P}_n := \langle i, \sigma_1^x, \sigma_1^z, \ldots, \sigma_n^x, \sigma_n^z \rangle, \tag{1}$$

where the stabilizer operators S_i constitute an Abelian subgroup of the Pauli group $\mathbf{P}_n$ of n qubits, generated by the Pauli matrices not containing -1. The ground state is a stabilizer code since it satisfies the condition

$$S_i|\mathrm{GS}\rangle = |\mathrm{GS}\rangle, \forall i, \tag{2}$$

and the excited states of H are gapped and correspond to error syndromes from the quantum information perspective

$$S_i|\Psi\rangle = -|\Psi\rangle. \tag{3}$$

The seminal example of topological stabilizer codes is the toric code [33]. There are basically two types of known topological stabilizer codes [13]. It is possible to study this type of homological error correcting code in many different situations and perform comparative studies [34]–[42]. TCC is another relevant example of a topological stabilizer code, with enhanced computational capabilities [1]–[3]. In particular, they allow the transversal implementation of Clifford quantum operations. The simplest lattice to construct them is a honeycomb lattice Λ shown in figure 1, where we place a spin-$\frac{1}{2}$ system at each vertex. There are two stabilizer operators per plaquette:

$$\begin{aligned} B_f^x &= \tau_1^x \tau_2^x \tau_3^x \tau_4^x \tau_5^x \tau_6^x, \\ B_f^y &= \tau_1^y \tau_2^y \tau_3^y \tau_4^y \tau_5^y \tau_6^y, \end{aligned} \tag{4}$$

$$H_{\mathrm{cc}} = -\sum_f (B_f^x + B_f^y), \tag{5}$$

where τ^ν's $(\nu = x, y)$ are usual Pauli operators. There exist six kinds of basic excitations. To label them, we first label the plaquettes with three colors: note that the lattice is three-valent and has three-colorable plaquettes. We call such lattices 2-colexes [3]. One can define color codes in any 2-colex embedded in an arbitrary surface. There exists a total of 15

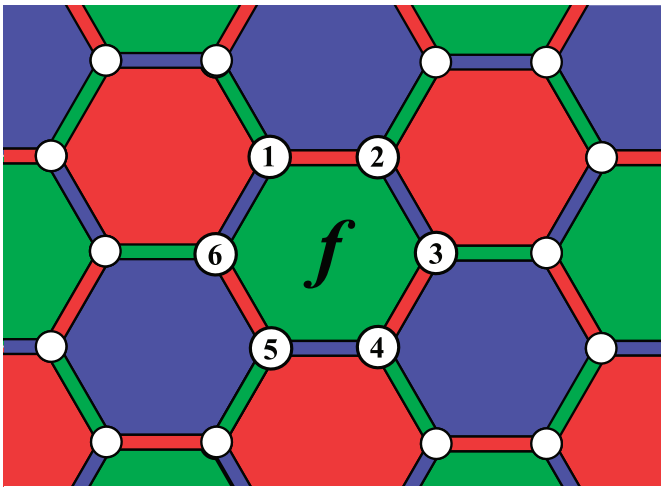

Figure 1. The hexagonal lattice is an example of a three-colorable lattice by faces, and also by edges. A TCC can be defined on it by associating two stabilizer operators for each plaquette (4).

nontrivial topological charges as follows. The excitation at a plaquette arises because of the violation of the stabilizer condition as in (3). Consider a rotation τ^y applied to a certain qubit. Since τ^y anti-commutes with plaquette operators B_f^x of neighboring plaquettes, it will put an excitation at a corresponding plaquette. Similarly, if we perform a τ^x rotation on a qubit, the plaquette operators B_f^y are violated. These are the basic excitations, two types of excitations for each colored plaquette. Regarding the color and type of basic excitations, different emerging excitations can be combined. The whole spectrum of excitations is shown in figure 2(a). Every single excitation is a boson by itself as well as the combination of two basic excitations with the same color. They form nine bosons. However, excitations of different colors and types have semionic mutual statistics as in figure 2(b). The excitations of different colors and types can also be combined. They form two families of fermions. Each family of fermions is closed under fusion, and fermions from different families have trivial mutual statistics. This latter property is very promising and will be the source of invisible charges as we will discuss in section 5. The anyonic charge sectors are in one-to-one correspondence with the irreducible representations (irreps) of the underlying gauge group, and the fusion corresponds to decomposition of the tensor product of irreps.

We describe all the above excitations in terms of representation of the gauge group of the TCC. Before that, let us make a convention for colors, which will be useful for subsequent discussions. We refer to colors by a bar operation $\bar{c}$ that transforms colors cyclically as $\bar{\mathrm{r}} = \mathrm{g}$, $\bar{\mathrm{g}} = \mathrm{b}$ and $\bar{\mathrm{b}} = \mathrm{r}$. The elements of the gauge group $\mathbf{Z}_2 \times \mathbf{Z}_2$ are {e, r, b, g}. Each excitation carries a topological charge. The corresponding topological charge can be labeled by the pair (q, χ), where $q \in \mathbf{Z}_2 \times \mathbf{Z}_2$ and χ is an irrep of this group [10]. We label them as $\chi_e(c) = \chi_c(c) = -\chi_c(\bar{c}) = 1$. Therefore, there are nine bosons labeled (c, χ_e), (e, χ_c) and (c, χ_c) and six fermions $(c, \chi_{\bar{c}})$ and $(c, \chi_{\bar{\bar{c}}})$. Taking into account the vacuum with trivial charge (e, χ_e), the color code has 16 topological charges or superselection sectors. Regarding the fusion process, fusion of the two charges (q, χ_c) and $(q', \chi_{c'})$ gives rise to tha charge $(qq', \chi_c\chi_{c'})$. Additionally, the braiding of the charge (q, χ_c) around the charge $(q', \chi_{c'})$ produces the phase $\chi_c(q')\chi_{c'}(q)$. An excitation

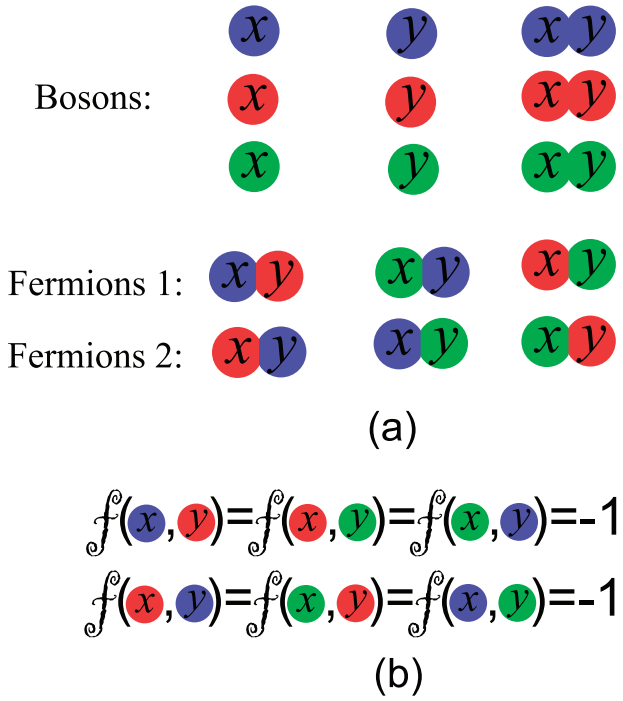

Figure 2. (a) Classification of excitations for the TCC model (5), nine bosons and two families of fermions (b) The nontrivial phase arising from the braiding of different charges.

at a c-plaquette has (c, χ_e) charge if $-B^x = B^y = 1$, (e, χ_c) charge if $B^x = -B^y = 1$ and (c, χ_c) charge if $B^x = B^y = -1$.

It is also possible to use both types of topological stabilizer codes, either toric codes or color codes, to go beyond homological operations. This corresponds to performing certain types of operations called code deformations, which may alter the topology of the surface, allowing an extension of the computational capabilities of these 2D codes [43]–[47].

Active error correction procedures are particularly interesting in the case of topological stabilizer codes. They give rise to connections with random statistical mechanical models like the random bond Ising model for the toric code [47] and new random three-body Ising models for color codes [48]. The whole phase diagram $p - T$ has been mapped out using Monte Carlo, which in particular gives the value of the error threshold p_c. This particular point can also be addressed using multi-critical methods [49]. There is experimental realization of topological error correction [50]. Without external active error correction, the effect of thermal noise is the most challenging problem in toric codes [51]–[56]. Finite-temperature effects of TO in color codes have also been studied [57].

In all, the type of entanglement exhibited by TCCs is very remarkable [58]–[64]. A very illustrative way to see this is using the connection of the ground state of topological codes with standard statistical models by means of projective measurements [7], [65]–[71]. For TCCs, this mapping yields the partition function of a three-body classical Ising model on triangular lattices [7]. This three-body model is the same as found in active error correcting techniques [48], but without randomness since there is no noise produced by external errors. This type of statistical mapping allows us to test whether different computational capabilities of

color codes correspond to qualitatively different universality classes of their associated classical spin models. Furthermore, generalizing these statistical mechanical models for arbitrary inhomogeneous and complex couplings, it is possible to study a measurement-based quantum computation with a color code state and we find that their classical simulatability remains an open problem. This is in sharp contrast with toric codes, which are classically simulable within this type of scheme [66].

2.2. The model

In nature, we find that interactions are usually two-body interactions. This is because interactions between particles are mediated by exchange bosons that carry the interactions (electromagnetic, phononic, etc) between two particles.

The problem that arises is that for topological models, such as the toric codes and color codes, their Hamiltonians have many-body terms (5). This can only be achieved by finding some exotic quantum phase of nature, like the fractional quantum Hall effect (FQHE), or by artificially engineering them somehow.

Here, we shall follow another route: try to find a two-body Hamiltonian on a certain 2D lattice such that it exhibits the type of TO found in toric codes and color codes. In this way, their physical implementation looks more accessible.

In fact, Kitaev [72] introduced a two-body model in the honeycomb lattice that gives rise to an effective toric code model in one of its phases. It is a two-body spin-$\frac{1}{2}$ model in a honeycomb lattice with one spin per vertex, and simulations based on optical lattices have been proposed [17].

The model features plaquette and string constants of motion. Furthermore, it is exactly solvable, a property that is related to the three-valency of the lattice where it is defined [72]–[78]. It shows emerging free fermions in the honeycomb lattice. If a magnetic field is added, it contains a non-abelian topological phase (although not enough for universal quantum computation). Interestingly, enough, another regime of the model gives rise to a four-body model, which is precisely an effective toric code model. A natural question arises: Can we get something similar for color codes? We give a positive answer in what follows.

Motivated by these physical considerations related to a typical scenario in quantum many-body physics, either condensed matter, AMO physics or the like, we will seek a quantum spin Hamiltonian with the following properties:

(i) One of its phases must be the TCC.

(ii) To have two sets of plaquette operators generating a $\mathbf{Z}_2 \times \mathbf{Z}_2$ local, i.e. gauge, symmetry.

(iii) To have string-nets and colored strings IOM as in the TCC, but in all coupling regimes.

Thus, the reasons for demanding these properties are to guarantee that the sought after model will host the TCC. For instance, property (i) means that we must be able to generate the 2D color code Hamiltonian consistently at some lowest order in PT. This we shall see in section 4.2. Likewise, properties (ii) and (iii) are demanded in order to have the fundamental signatures regarding gauge symmetry and constants of motions associated with TCCs. Note that we have not demanded that the model be exactly solvable. This is a mathematical requisite, rather than physical. We leave the door open for considering larger classes of models beyond exactly solvable models, which may be very interesting and contain new physics. For example, according to those properties, it would be possible to have models with a number of IOMs that

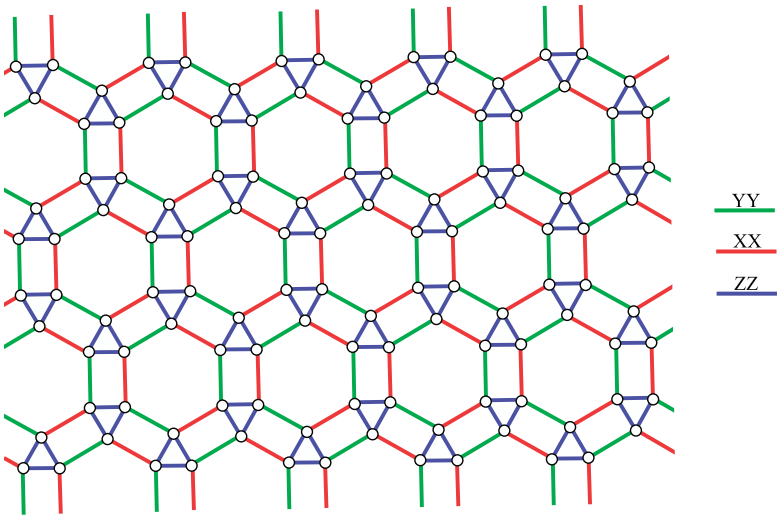

Figure 3. A lattice with coordination number 4 where the two-body quantum lattice Hamiltonian for the color codes is defined according to spin–spin interactions coded by the colors of the links, as in (6). A plaquette can be distinguished by an inner hexagon, an outer hexagon and six blue triangles between them.

scale linearly with N, the number of spins or qubits. Thus, the Kitaev model has a number of IOMs of $\frac{1}{2}N$.

Our purpose is to present first the two-body quantum Hamiltonian in 2D [10], and then to analyze diverse possible mappings in later sections, such as using bosonic and fermionic degrees of freedom. The analysis of the set of IOMs will also play a crucial role in the understanding of our model as we shall see in section 3.

It is a two-body spin-$\frac{1}{2}$ model in a 'ruby' lattice as shown in figure 3. We place one spin per vertex. Links come in three colors, each color representing a different interaction.

$$H = -\sum_{\langle i,j\rangle} J_w \sigma_i^w \sigma_j^w, \qquad w = \begin{cases} x, & \text{red links,} \\ y, & \text{green links,} \\ z, & \text{blue links.} \end{cases} \tag{6}$$

For a suitable coupling regime, this model gives rise to an effective color code model. Furthermore, it exhibits new features, many of them not present in honeycomb-like models:

- Exact topological degeneracy in all coupling regimes (4^g for genus g surfaces).
- String-net IOM.
- Emergence of three families of strongly interacting fermions with semionic mutual statistics.
- $\mathbf{Z}_2 \times \mathbf{Z}_2$ gauge symmetry. Each family of fermions sees a different $\mathbf{Z}_2$ gauge subgroup.

3. String operators and integrals of motion

We can construct IOM, $I \in \mathbf{P}_n$, $[H_{\rm cc}, I] = 0$, following a pattern of rules assigned to the vertices of the lattice, as shown in figure 4. These rules are constructed to attach a Pauli operator of type

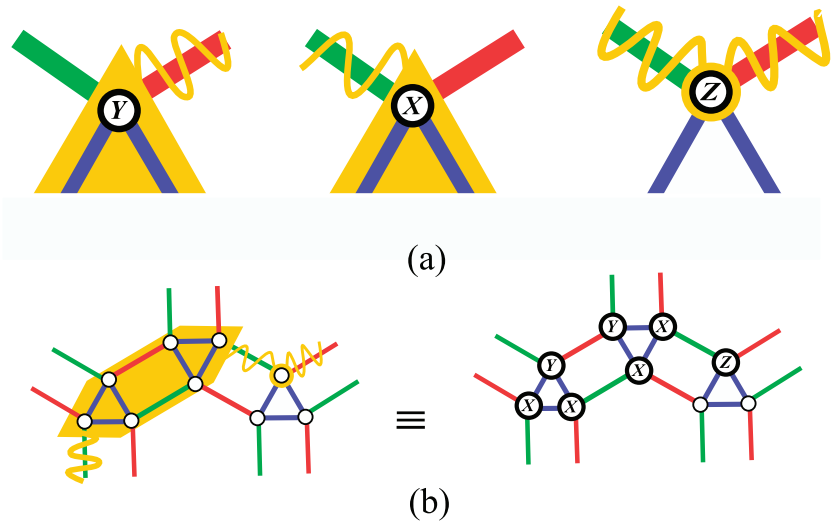

Figure 4. (a) A diagrammatic representation of the local structure of the IOM of the two-body Hamiltonian (6). The colored links represent different spin–spin interactions. (b) An example of contribution of Pauli operators in a string.

σ_i^x, σ_i^y or σ_i^z to each of the vertices i. The lines around the vertices, either wavy lines or direct lines, are pictured in order to join them along paths of vertices in the lattice that will ultimately translate into products of Pauli operators, which will become IOMs. Clearly, σ_i^z operators are distinguished from the rest. The contribution of each qubit in the string operator is determined in terms of how it appears in the string. Its contribution may be determined by the outgoing red and green links, which have the qubit as their end point in the string. In this case, the σ^x or σ^y Pauli operators contribute to the string IOM. If a typical qubit is crossed only by a wavy line as shown in figure 4(a), it contributes a σ^z Pauli operator in the string. To have a clear picture of string operators, a typical example has also been shown in figure 4(b). A part of the string is shown on the left and its expression will be the product of Pauli operators, which have been inserted in open circles on the right. With such definitions for string operators and their supports on the lattice, we now turn to analyzing the relevance of strings to the model. In particular, we will construct elementary string operators with the local symmetry of the model. Therefore, in this way, we are representing the local structure of the IOMs of our two-body Hamiltonian (5). We will illustrate them with several examples of increasing complexity. The ground state of a lattice model described by the Hamiltonian (5) is a superposition of all closed colored strings. Indeed, it is invariant under any deformations of colored strings as well as splitting of a colored string into other colors. In other words, the ground state is a string-net condensed state and supports TO. The gauge group related to this TO is $\mathbf{Z}_2 \times \mathbf{Z}_2$. Such symmetry of the TCC can be realized via defining a set of closed string operators on the ruby lattice. We shall verify the gauge symmetry by identifying a set of string operators on the lattice of figure 3.

Let us start by constructing the elementary string IOM as shown in figure 5. They are denoted as $I = A, B, C$. They are closed since they have no endpoints left. The elementary closed strings are plaquettes. By a plaquette we mean an inner hexagon and an outer hexagon with six triangles in between. For a given plaquette, it is possible to attach three string operators. For each closed string, the contributions of Pauli operators are determined based on outgoing

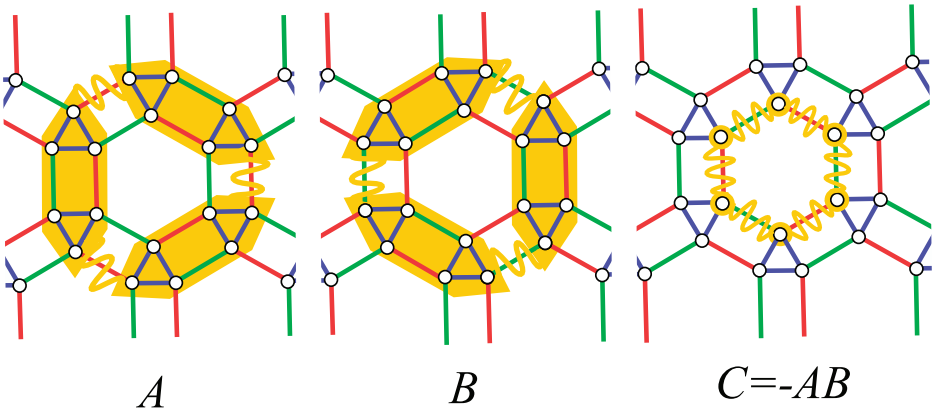

Figure 5. Schematic drawing of the plaquette IOMs according to the local rules in figure 4. There are three IOMs denoted as A, B and C, but only two of them are independent. This corresponds to the symmetry $\mathbf{Z}_2 \times \mathbf{Z}_2$ of the model.

red and green links or wavy lines as in figure 4. Let V_f stand for a set of qubits on a plaquette. Note that each plaquette contains 18 qubits corresponding to six triangles around it. For the first plaquette operator in figure 5, we can write its explicit expression in terms of Pauli matrices as $S_f^A = \prod_{i\in V_f} \sigma_i^{\nu}$, where f denotes the plaquette and $\nu = x$, y, depending on outgoing red or green links, respectively. Similarly, the second plaquette operator has the expression $S_f^B = \prod_{i\in V_f} \sigma_i^{\nu}$. The third string is only a closed wavy string that coincides with the inner hexagon of the plaquette. Its expression is $S_f^C = \prod_{i\in V_h} \sigma_i^z$, where V_h stands for six qubits on the inner hexagon. The three closed strings described above are not independent. Using the Pauli algebra, it can immediately be checked that they satisfy $S_f^C = -S_f^A S_f^B$. Thus, there exist two independent IOMs per plaquette: this is the $\mathbf{Z}_2 \times \mathbf{Z}_2$ local symmetry of the model Hamiltonian (6).

Plaquette operators commute with each other and with any other IOM. If an IOM corresponds to a nontrivial cycle c, it is possible to find another IOM that anti-commutes with it, namely one that corresponds to a cycle that crosses c' once. Thus, IOMs obtained from nontrivial cycles are not products of plaquette operators.

Each string operator squares identity, since we are working with qubits. Plaquette operators corresponding to different plaquettes commute with each other and also with terms in Hamiltonian in (6) since they share zero or even numbers of qubits. Therefore, the closed strings with the underlying symmetry obtained above define a set of IOM. The number of IOMs is exponentially increasing. Let $3N$ be the total number of qubits, so the number of plaquettes will be $\frac{N}{2}$. Regarding the gauge symmetry of the model, the number of independent plaquette operators is N. This implies that there are 2^N IOM and this allows us to divide the Hilbert space into 2^N sectors being eigenspaces of plaquette operators. However, for a closed manifold, for example a torus, all plaquette operators cannot be independently set as $+1$ or -1 because they are subject to some constraints. All other closed string operators that are homologous to zero, i.e. they are homotopic to the boundary of a plaquette, are just the product of these elementary plaquette operators. It is natural that all of them are topologically equivalent up to a deformation and commute with the Hamiltonian of the model.

The most general configuration that we may have is shown in figure 6. We call them string-nets IOM since in the context of our model, they can be thought of as the string-nets introduced to characterize TOs [79]. The key feature of these IOMs is the presence of branching points

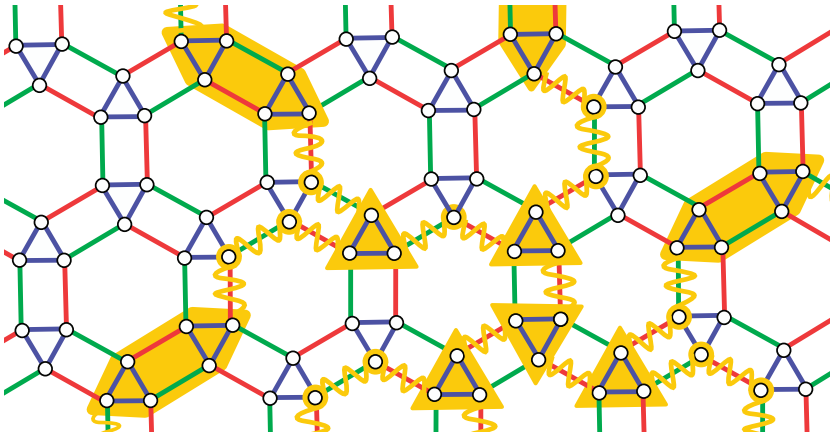

Figure 6. An example of a string-net IOM. Note the presence of branching points located around blue triangles of the lattice. This is a remarkable difference with respect to honeycomb models like the Kitaev model.

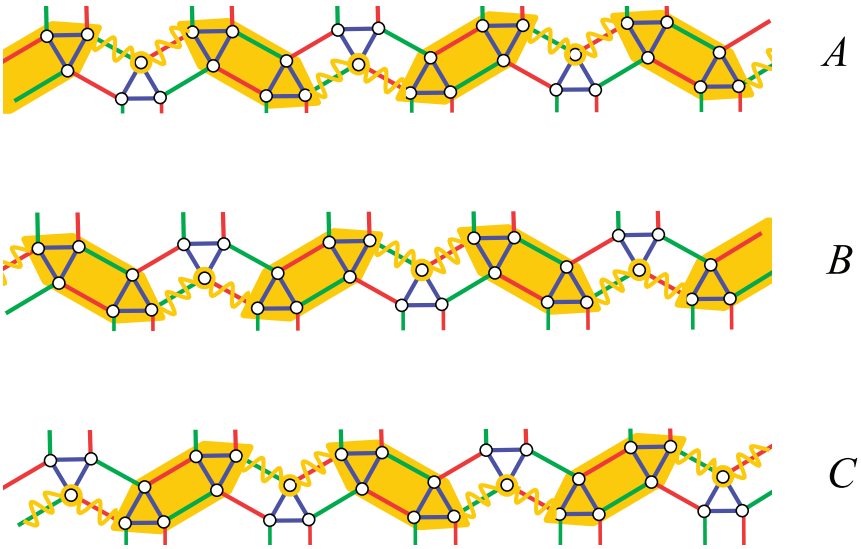

Figure 7. Examples of standard string configurations of IOMs, i.e. without branching points. For each path, we can in principle make three different assignments of IOMs, but again only two of them are independent as with plaquette IOMs. This is another manifestation of the $\mathbf{Z}_2 \times \mathbf{Z}_2$ symmetry of the model.

located at the blue triangles of the lattice. This is remarkable and is absent from honeycomb two-body models like the Kitaev model. When the string-nets IOM are defined on a simply connected piece of lattice they are products of plaquette operators. More generally, they can be topologically nontrivial and independent of plaquette operators.

As a special case of IOMs, we have string configurations, i.e. paths without branching points. They correspond to the different homology classes of the manifold where the lattice is embedded, and are needed for characterization of the ground state manifold. Some examples are shown in figure 7. They may be open or closed, depending on whether they have endpoints or

not, respectively. Strings IOM are easier to analyze. String-nets IOM are products of strings IOM. For a given path, there exist three different strings IOM. These are denoted as A, B and C in figure 7. We must introduce generators for the homology classes defining closed manifold. Homology classes of the torus are determined by realizing two nontrivial loops winding around the torus. In Kitaev's model, there are only two such independent nontrivial closed loops. However, the specific construction of the lattice and the contribution of the color make it possible to define for each homology class of the torus two independent nontrivial loops. These closed strings are no longer a combination of the plaquettes defined above. Let S_μ^A stand for such a string, where A and μ denote the type and homology class of the string. For each homology class of the manifold, we can realize three different types of string operators depending on how the vertices of the lattice are crossed by the underlying string. Each qubit crossed by the string contributes a Pauli operator according to the rules in figure 4. Again, using Pauli algebra we can see that only two of them are independent, as with the plaquette IOMs.

$$(-1)^{\frac{t}{2}} S_\mu^A S_\mu^B S_\mu^C = 1, \tag{7}$$

where t is the number of triangles on the string. To distinguish properly the three types we have to color the lattice. We could already use the colors to label strings. Strings are then red, green or blue. This is closely related to the TCC [1, 10]. The latter relation shows that each string can be constructed of two other homologous ones, which is exactly the expression of the $\mathbf{Z}_2 \times \mathbf{Z}_2$ gauge symmetry. Each non-contractible closed string operator of any homology commutes with all plaquette operators and with terms appearing in the Hamiltonian, so they are constants of motion. But they do not always commute with each other. In fact, if the strings cross once, then

$$\left[S_\mu^r, S_\nu^r\right] = 0, \tag{8}$$

but

$$\{S_\mu^r, S_\nu^{r'}\} = 0. \tag{9}$$

The latter anti-commutation relation is the source of exact topological degeneracy [80] of the model independent of phase we are analyzing.

4. A gapped phase: the TCC

4.1. Non-perturbative picture

In this subsection, we propose that the ruby lattice is connected to the 2-colex even at the non-perturbative level. Then, in subsequent sections, we verify this using quantitative methods. From the previous discussion on IOMs, we have already seen a connection with the TCCs. Now, we want to see how the different strings introduced above are related to coloring of the lattice. To this end, consider the closed strings A, B and C in figure 5. The closed strings A and B can be visualized as a set of *red* and *green* links, respectively. With such a visualization, we put forward the next step to color the inner hexagons of the ruby lattice: a colored link, say red, connects the red inner hexagons. Accordingly, other inner hexagons and links can be colored, and eventually we are left with a colored lattice. The emergence of the TCC is beautifully pictured in figure 8. Geometrically, it corresponds to shrinking the blue triangles of the original lattice into points,

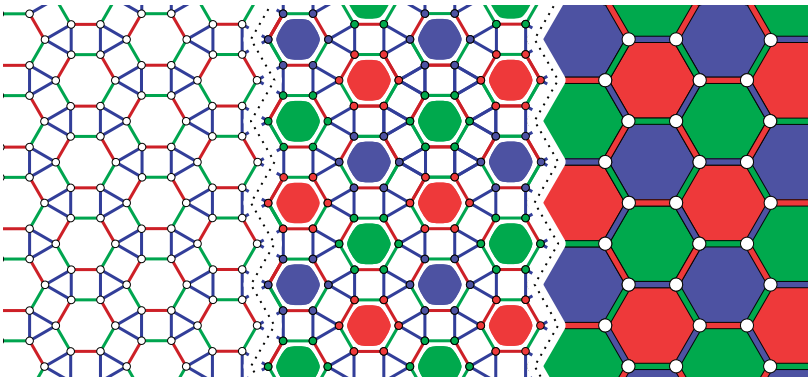

Figure 8. The three stages showing the emergence of the TCC: (left) the original lattice for the two-body Hamiltonian (6). The colors in the links denote the type of spin–spin interactions; (middle) a different coloring of the lattice is introduced based on the property that the hexagons are 3-colorable, as well as the vertices; (right) the hexagonal lattice is obtained by shrinking to a point the blue triangles of the original lattice, which become sites in the final hexagonal lattice. This corresponds to the strong coupling limit in (15).

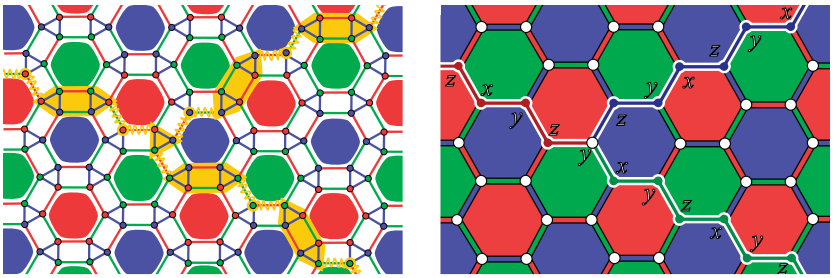

Figure 9. An illustration of the correspondence between (a) strings on the ruby lattice, corresponding to a non-perturbative picture, and (b) colored strings on the effective honeycomb lattice.

which will be referred to as sites of a new emerging lattice, see figure 8 (left). Thus, we realize that the inner hexagons and vertices of the model are colorable, see figure 8 (middle): if we regard blue triangles as the sites of a new lattice, we get a honeycomb lattice, see figure 8 (right). In fact, the model could be defined for any other 2-colex, not necessarily a hexagonal lattice.

Connection to the 2-colexes can be further explored by seeing how strings on the ruby lattice correspond to the colored strings on the effective honeycomb lattice. To this end, consider a typical string-net on the ruby lattice as shown in figure 9(a). This corresponds to a non-perturbative picture of the IOMs of the model. The fat parts of the string-net connect two inner hexagons with the same color. In this way, the corresponding string-net on the effective lattice can be colored as in figure 9(b). The color of each part of the string-net on the effective honeycomb lattice is determined by finding out to which colored inner hexagons on the ruby

lattice it connects. Three colored strings cross each other at a branching point, and its expression in terms of Pauli matrices of sites is given by the product of Pauli operators written adjacent to the sites. How they are determined will be clear soon.

It is possible to use colors to label the closed strings on the honeycomb lattice. Before that, let us use a notation for Pauli operators acting on effective spins of honeycomb lattice τ^{α}, where $\alpha = x, y, z$. We indicate the label α as $c|c := z$, $\bar{c}|c := x$ and $\bar{\bar{c}}|c := y$, where we are using a bar operator. To each c-plaquette, we attach three operators each of one color. Let $B_f^{c'}$ denote such operators, where the lower and upper indices stand for the c-plaquette f and the color of the closed string attached to the plaquette, respectively. With these notations, the plaquette operators read as follows:

$$B_f^{c'} = \prod_{v \in f} \tau_v^{c'|c}, \tag{10}$$

where the product runs over all vertices of the c-plaquette f in the honeycomb lattice in figure 8(c). Thus, we can write the explicit expression of operators as follows:

$$\begin{aligned} B_f^x = B_f^{\bar{c}} &= \prod_{v \in f} \tau_v^{\bar{c}|c}, \\ B_f^y = B_f^{\bar{\bar{c}}} &= \prod_{v \in f} \tau_v^{\bar{\bar{c}}|c}, \\ B_f^z = -B_f^c &= -\prod_{v \in f} \tau_v^{c|c}. \end{aligned} \tag{11}$$

All these plaquette operators are constants of motion. Again, we can realize the gauge symmetry $\mathbf{Z_2} \times \mathbf{Z_2}$ through the relation $B_f^x B_f^y B_f^z = 1$. On a compact manifold, for example on the torus, all plaquettes are not independent. They are subject to the following constraint:

$$\prod_{f \in \Lambda} B_f^c = (-1)^{N/2}, \tag{12}$$

where the product runs over all plaquettes f in the lattice Λ, and N is the total number of plaquettes.

We can also realize non-contractible strings on the effective lattice which are rooted in the topological degeneracy of the model. They are just the IOMs in figure 7 when reduced on the effective honeycomb lattice. Once the inner hexagons of the ruby lattice are colored, they correspond to colored strings as in figure 9. Let S_μ^c stands for such a string, where indices μ and c denote the homology and color of the string, respectively. This string operator is a tensor product of Pauli operators of qubits lying on the string. Namely, the string operator is

$$S_\mu^c = \prod_{v} \tau_v^{c'|c}. \tag{13}$$

The contribution of each qubit is determined by the color of the hexagon that the string turns on (see figure 10). For example in the string S_1 shown in figure 10, the color of the plaquettes appearing in (13) is marked by light circles. With this definition for string operators, the contribution of Pauli operators in the string-net to the effective lattice in figure 9(b) is reasonable. Non-contractible colored strings are closely related to the topological degeneracy of the model, since they commute with color code Hamiltonian (5) being IOM, but not always

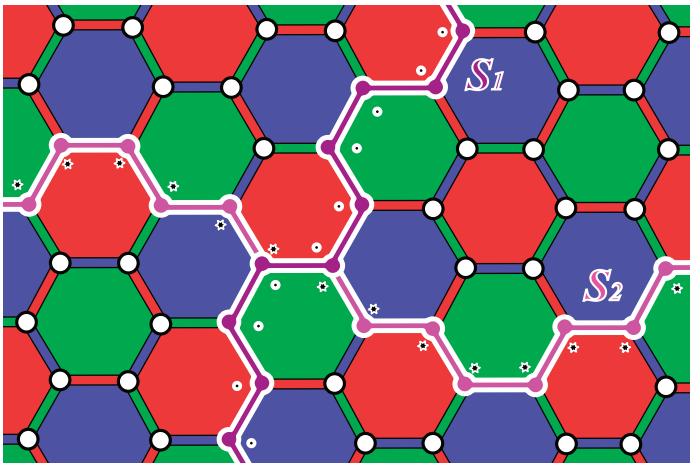

Figure 10. A piece of effective lattice. The strings S_1 and S_2 correspond to different homology classes of the manifold. Their expressions in terms of Pauli operators are given by their associated color and how they turn on plaquettes on the lattice.

with each other. In fact, if two strings differ in both homology and color, they anti-commute; otherwise they commute. For example, let us consider two non-contractible closed strings S_1 and S_2 corresponding to different homologies of the torus. As shown in figure 10, they share two qubits. First, suppose both strings are of blue type. The contribution of the Pauli operators of these two qubits in string S_1 is $\tau_1^y \tau_2^x$, while for string S_2 the contribution is $\tau_1^x \tau_2^y$ implying $[S_1^b, S_2^b] = 0$. Then, let S_2 be a green string. In this case, the contribution of qubits will be $\tau_1^y \tau_2^z$, which explicitly shows that $\{S_1^b, S_2^g\} = 0$. The interplay in (7) can be translated into an interplay between color and homology as follows:

$$(-1)^{\frac{s}{2}} S_\mu^c S_\mu^{\bar{c}} S_\mu^{\bar{\bar{c}}} = 1, \tag{14}$$

where s is the number of sites on the string. This interplay makes the ground state subspace of the color code model a string-net condensed phase.

4.2. Degenerate perturbation theory: the Green function formalism

In this subsection, we put the above correspondence between the original two-body lattice Hamiltonian and the color code model on a quantitative level. In fact, there is a regime of coupling constants in which one of the phases of the two-body Hamiltonian reproduces the TCC many-body structure and physics. In particular, we show that this corresponds to the following set of couplings in the original two-body Hamiltonian

$$J_x, J_y, J_z > 0, \quad J_x, J_y \ll J_z, \tag{15}$$

that is, a strong coupling limit in J_z. The TCC effectively emerges in this coupling regime. This can be seen using degenerate PT in the Green function formalism. Let $H = H_0 + V$ be a Hamiltonian describing a physical system with two-body interaction, and we regard the $\|V\|$, the norm of V, as very small in comparison with the spectral gap of *unperturbed* H_0. We also suppose that H_0 has a degenerate ground-subspace that is separated from the excited states by a gap Δ. The effect of V will be to break the ground state degeneracy in some order of

perturbation. Now the interesting question is whether it is possible to construct an effective Hamiltonian, H_{eff}, which describes the low-energy properties of the perturbed Hamiltonian H. The effective Hamiltonian arises at orders of perturbation that break the ground state degeneracy. From the quantum information perspective the Hamiltonian H acts on the physical qubits, while the effective Hamiltonian acts on the logical qubits projected down from the physical qubits.

We will clarify how the many-body Hamiltonian in (5) will present an effective description of low-lying states of the two-body Hamiltonian (6). We use the perturbation about the Hamiltonian in (6) considering the coupling regime (15). Here, the qubits on the triangles are physical qubits, and logical qubits are those living at the vertices of the 2-colex. We refer to triangles as sites, since they correspond to the vertices of the 2-colex. Thus, a triangle will be shown by index v and its vertices by Latin indices i, j. In fact, the low-lying spectrum of the two-body Hamiltonian encodes the following projection from the physical qubits to the logical ones at each site:

$$P_v = |\Uparrow\rangle\langle\uparrow\uparrow\uparrow| + |\Downarrow\rangle\langle\downarrow\downarrow\downarrow|, \tag{16}$$

where $|\Uparrow\rangle$ and $|\Downarrow\rangle$ stand for the two states of the logical qubit at site v, and $|\uparrow\rangle$ ($|\downarrow\rangle$) is the usual up (down) states of a single spin in computational bases.

To this end, we split the two-body Hamiltonian into two parts. The unperturbed part is $H_0 = -J_z \sum_{\text{b-link}} \sigma_i^z \sigma_j^z$. In the limit of strong Ising interaction, the system is polarized. The interactions between neighboring qubits on different triangles are included in V. They are $\sigma_i^x \sigma_j^x$ and $\sigma_i^y \sigma_j^y$ corresponding to red and green links in figure 3, respectively. Hence, the transverse part of the Hamiltonian is

$$V = -J_x \sum_{\text{r-link}} \sigma_i^x \sigma_j^x - J_y \sum_{\text{g-link}} \sigma_i^y \sigma_j^y. \tag{17}$$

In the case when $J_z \gg J_x, J_y$ the low-lying excitations above the fully polarized state can be treated perturbatively.

The unperturbed part of the Hamiltonian, H_0, has a highly degenerate ground space because, for each triangle, the two fully polarized states $|\uparrow\uparrow\uparrow\rangle$ and $|\downarrow\downarrow\downarrow\rangle$ have the same energy. The ground state subspace is spanned by all configurations of such polarized states. Let N be the number of triangles of the lattice. The ground state energy is $E_0^{(0)} = -3NJ_z$ and the dimension of the ground space of the H_0 or ground state degeneracy reads $g_0 = 2^N$. The first excited state is produced by exciting one of the triangles and has energy $E_1^{(0)} = (-3N+4)J_z$ with degeneracy $g_1 = 6N2^{N-1}$. The second excited state has energy $E_1^{(0)} = (-3N+8)J_z$ with degeneracy $g_2 = 18N(N-1)2^{N-2}$, and so on and so forth.

We analyze the effect of V on the ground state manifold by using the degenerate PT [81] in couplings J_x and J_y. We are interested in how ground state degeneracy is lifted by including the interaction between triangles perturbatively. Let $\mathcal{L}$ stand for the ground state manifold with energy $E_0^{(0)}$ and let P be the projection onto the ground state manifold $\mathcal{L}$. The projection is obtained from the degenerate ground states as follows:

$$P = \prod_{v\in\Lambda} P_v, \quad P_v = |\Uparrow\rangle\langle\uparrow\uparrow\uparrow| + |\Downarrow\rangle\langle\downarrow\downarrow\downarrow|. \tag{18}$$

Using the projection and Green's function, we can calculate the effective Hamiltonian at any order of PT. The eigenvalues of the effective Hamiltonian H_{eff} appear as the poles of the Green function $G(E) = P[1/(E-H)]P$. The effect of perturbation can be recast into the

self-energy $\Sigma(E)$ by expressing Green's function as $1/(E - E_0^{(0)} - \Sigma(E))$. Hence, the effective Hamiltonian will be

$$H_{\text{eff}} = \sum_{l=0}^{\infty} H_{\text{eff}}^{(l)} = E_0^{(0)} + \Sigma(E). \tag{19}$$

The self-energy can be represented in terms of Feynman diagrams and can be computed for any order of perturbation:

$$\Sigma(E) = PV \sum_{n=0}^{\infty} \mathcal{U}^n P, \tag{20}$$

where $\mathcal{U} = [1/(E - H_0)](1 - P)V$. The energy E can also be expanded at different orders of perturbation, $E = E_0^{(0)} + \sum_{l=1}^{\infty} E_0^{(l)}$. Now, we are in a position to determine different orders of perturbation. Each term of V acts on two neighboring physical qubits of different triangles. At a given order of PT, there are terms that are the products of σ^x and σ^y acting on the ground state subspace. Each term, when it acts on the ground state manifold, brings the ground state into an excited state. However, there may be a specific product of the σ^x and σ^y that takes the ground state into itself, i.e. preserves the polarized configurations of triangles.

At zeroth order, the effective Hamiltonian will be trivial $H_{\text{eff}}^{(0)} = E_0^{(0)}$. The first-order correction is given by the operator

$$H_{\text{eff}}^{(1)} = PVP. \tag{21}$$

The effect of V is to move the states out of the ground state manifold because each term, either $\sigma^x\sigma^x$ or $\sigma^y\sigma^y$, flips two qubits, causing two triangles to be excited, i.e. $VP = P_2VP$, where the operator P_2 is the projection to the second excited state manifold. Therefore, $PVP = 0$, and there is no first-order correction to the ground state energy.

The second-order correction to the ground state will be the eigenvalues of the following operator:

$$H_{\text{eff}}^{(2)} = PVG'(E_0^{(0)})VP + PVP, \tag{22}$$

where the operator $G'(E) = 1/(E - H_0)$ is the unperturbed Green function and the superscript prime stands for the fact that its value is zero when it acts on the ground state. The second-order correction only shifts the ground state energy, and therefore, the second-order effective Hamiltonian acts trivially on the ground state manifold,

$$H_{\text{eff}}^{(2)} = 3N \frac{J_x^2 + J_y^2}{-8J_z} P. \tag{23}$$

In fact the first V flips the qubits and the second V flips them back. As we go to higher order of PT, the terms become more and more complicated. However, if the first-order is zero as in our case, the terms becomes simpler. Thus, the third order of perturbation will be zero and will leave corrections to energy and ground state intact:

$$H_{\text{eff}}^{(3)} = PV(G'(E_0^{(0)})V)^2 P = 0. \tag{24}$$

The fourth order of PT contributes the following expression to the correction of the ground state manifold:

$$H_{\text{eff}}^{(4)} = PV(G'(E_0^{(0)})V)^3 P - E_0^{(2)} PV(G'(E_0^{(0)}))^2 VP, \tag{25}$$

where $E_0^{(2)}$ is the second-order correction to the ground state energy obtained in (23). The first term includes four V and must act in the ground state in which the last V returns the state to the ground state manifold. The second term is like the second order. There are many terms that must be calculated. However, since the fourth order only gives a shift to the ground state energy, we do not need them explicitly. Hence, we can skip the fourth order. Fifth-order correction yields terms that each contain an odd number of V, so it gives zero contribution to the effective Hamiltonian.

The sixth order of perturbation leads to the following long expression:

$$\begin{aligned} H_{\text{eff}}^{(6)} = {} & PV(G'(E_0^{(0)})V)^5P - E_0^{(4)}PV(G'(E_0^{(0)}))^2VP + (E_0^{(2)})^2PV(G'(E_0^{(0)}))^3VP \\ & - E_0^{(2)}PV(G'(E_0^{(0)}))^2V(G'(E_0^{(0)})V)^2P - E_0^{(2)}PVG'(E_0^{(0)})V(G'(E_0^{(0)}))^2VG'(E_0^{(0)})VP \\ & - E_0^{(2)}PV(G'(E_0^{(0)})V)^2(G'(E_0^{(0)}))^2VP. \end{aligned} \tag{26}$$

Apart from the first term, other terms contain two or four V and, as we have discussed in the preceding paragraphs, they only contribute a shift in the ground state energy. However, the first term gives the first nontrivial term breaking in part the ground state degeneracy. In the sixth-order correction, there are some terms that are the products of $\sigma^x\sigma^x$ and $\sigma^y\sigma^y$ associated with the red and green links of the ruby lattice. Some particular terms, as seen below, may map the ground state subspace into itself. For instance, consider the following product of links around an inner hexagon:

$$\prod_{\langle i,j\rangle}\sigma_i^w\sigma_j^w = \pm\prod_{i\in V_h}\sigma_i^z, \tag{27}$$

where the first product runs over three red and three green links, making an inner hexagon, V_{h} stands for the set of its vertices and the prefactor $\pm$ depends on the ordering of links in the product. The action of a σ^z on one vertex (qubit) of a triangle encodes a logical τ_v^z operator acting on the associated vertex of lattice Λ. This can explicitly be seen from the following relation:

$$\tau_v^z = P_v\sigma^zP_v = |\Uparrow\rangle\langle\Uparrow| - |\Downarrow\rangle\langle\Downarrow|, \tag{28}$$

where σ^z acts on one of the vertices of a triangle and P_v is the projection defined in (16). Thus, the expression of (27) can be related to the plaquette operator $B_f^z = -\prod\tau_v^z$, where the index f denotes a plaquette of that effective lattice Λ as in figure 1 and the product runs over six sites around it. Now we proceed to pick up the sixth-order correction to the ground state manifold. There are many terms that must be summed. Sixth-order correction up to a numerical constant contributes the following expression to the effective Hamiltonian:

$$H_{\text{eff}}^{(6)} = \text{constant} - \delta\frac{J_x^3J_y^3}{J_z^5}\sum_f B_f^z, \tag{29}$$

where δ is a positive numerical constant arising from summing 720 terms related to the order of product of six links around an inner hexagon of the ruby lattice. Although its exact numerical value is not important, knowing its sign is essential for our subsequent discussions. As is clear from the first term in (26), five Green's functions and six V in the perturbation contribute a minus sign to the expression. This minus sign together with the sign appearing in (27) makes the coefficient δ a positive constant. Now it is simple to realize how the vectors in the ground state manifold are rearranged. Trivially, all plaquette operators B_f^z commute

with each other and their eigenvalues are ± 1. All polarized vectors in $\mathcal{L}$ are eigenvectors of the effective Hamiltonian emerging at sixth order. But those are ground states of the effective Hamiltonian in (29) which are eigenvectors of all plaquette operators B_f^z with eigenvalue +1. Thus, the highly degenerate ground state of the unperturbed Hamiltonian is broken in part. The same plaquette operators B_f^z also appear at higher order of perturbation, for example, at the eighth order. Instead of giving the rather lengthy expression of the eighth-order correction, we keep only terms resulting in the plaquette operators shown below:

$$H_{\text{eff}}^{(8)} = \text{constant} - \beta \frac{J_x^5 J_y^3 + J_x^3 J_y^5}{J_z^7} \sum_f B_f^z, \tag{30}$$

where $\beta > 0$. This term is added to the one in (29) to give the effective Hamiltonian up to eighth order, but the ground state structure remains unchanged. Further splitting in the ground state manifold is achieved by taking into account the ninth order of perturbation. The expression of the ninth order is very lengthy. However, the first term of the expression containing nine V gives some terms that are capable of mapping the ground state manifold onto itself in a nontrivial way. These terms map a polarized triangle, say an up triangle, to a down one. Indeed, when one or two qubits of the polarized triangle get flipped, its state is excited. However, flipping three qubits of the triangle returns the ground state back onto itself. This process encodes τ^x and τ^y logical operators acting on logical qubits arising through the projection. Let σ_1^x, σ_2^x and σ_3^y act on three qubits of a triangle. The encoded τ^y operator will be

$$\tau_v^y = P_v \sigma_1^x \sigma_2^x \sigma_3^y P_v = -\mathrm{i}|\Uparrow\rangle\langle\Downarrow| + \mathrm{i}|\Downarrow\rangle\langle\Uparrow|. \tag{31}$$

If σ_1^x, σ_2^y and σ_3^y act on three qubits of a triangle, the encoded τ^x logical operator will be

$$-\tau_v^x = P_v \sigma_1^x \sigma_2^y \sigma_3^y P_v = -|\Uparrow\rangle\langle\Downarrow| - |\Downarrow\rangle\langle\Uparrow|. \tag{32}$$

As we have already pointed out, a plaquette of the ruby lattice is made up of an inner hexagon, an outer hexagon and six blue triangles. It is possible to act on the polarized space of the blue triangles by making two different combinations of 9-link interactions: (i) Applying 6-link interactions on the outer hexagon (three of them of XX type and another three of YY type), times 3-link interactions of red type on the inner hexagon. Note that every vertex of the blue triangles in the plaquette gets acted upon by these 9-link interactions. The resulting effective operator is of type τ^y due to (31). (ii) Applying 6-link interactions on the outer hexagon, times 3-link interactions of green type. Then, the resulting effective operator is of type τ^x due to (32).

The effective Hamiltonian at this order then reads

$$\begin{aligned} H_{\text{eff}}^{(9)} &= PV(G'(E_0^{(0)})V)^8 P + \cdots \\ &= \text{constant} - \gamma \frac{J_x^6 J_y^3}{J_z^8} \sum_f B_f^y - \gamma \frac{J_x^3 J_y^6}{J_z^8} \sum_f B_f^x. \end{aligned} \tag{33}$$

Again, the sign of the coefficient γ is important. Nine Vs, six τ^x or τ^y and eight Green's functions imply that the γ must have positive sign.

Putting together all the above obtained corrections leads to an effective Hamiltonian encoding the color code as its ground state [1, 58]. Therefore, up to constant terms, the effective Hamiltonian reads as follows:

$$H_{\text{eff}} = -k_z \sum_f B_f^z - k_x \sum_f B_f^x - k_y \sum_f B_f^y, \tag{34}$$

where k_z, k_x and k_y are positive coefficients arising at different orders. Since $B_f^x B_f^y = B_f^z$, the above effective Hamiltonian is just the many-body Hamiltonian of the color code as in (1). The terms appearing in the Hamiltonian mutually commute, so the ground state will be the common eigenvector of plaquette operators. Since each plaquette operator squares identity, the ground state subspace, $\mathcal{C}$, is spanned by vectors that are common eigenvectors of all plaquette operators with eigenvalue +1, that is,

$$\mathcal{C} = \{|\psi\rangle : B_f^x|\psi\rangle = |\psi\rangle,\ B_f^y|\psi\rangle = |\psi\rangle;\ \forall f\}. \tag{35}$$

The group of commuting boundary closed string operators can be used as an alternative way to find the terms appearing in the effective Hamiltonian [82]. As we pointed out in the preceding section, the nonzero contributions from various orders of PT result from the product of red and green links, which preserve the configurations of the polarized triangles, i.e. the maps ground the state manifold onto itself. For instance, consider the elementary plaquette operator A corresponding to a closed string in figure 5. Each triangle contributes $\sigma^y\sigma^y\sigma^x$ to the expression of the operator that is projected to τ^x as in (32). Thus, the effective representation of plaquette operator reads as follows:

$$PS_f^A P \to B_f^x. \tag{36}$$

Plaquette operators S_f^B and S_f^C can also be recast into the following effective forms:

$$PS_f^B P \to B_f^y, \quad PS_f^C P \to -B_f^z. \tag{37}$$

These are lowest order contributions to the effective Hamiltonian we obtained in (34). Higher order of perturbation will be just the product of effective plaquette operators. The nontrivial strings winding around the torus will also have effective representations and appear at higher orders of perturbation. In general, every string-net IOM on the ruby lattice is projected on an effective one as in figure 9.

5. Bosonic mapping

As we stated in section 3, one of the defining properties of our model is the existence of nontrivial IOM, called string-nets. As a particular example, Kitaev's model on the honeycomb lattice has strings IOMs, but not string-nets. We are interested in models in which the number of IOMs is proportional to the number of qubits in the lattice, i.e.

$$I = \eta N_q, \tag{38}$$

where I is the number of IOMs, N_q is the number of qubits (spins) in the lattice, and η is a fraction: $\eta = \frac{1}{2}$ for the Kitaev model [72] and $\eta = \frac{1}{3}$ for our model in (6) [10]. The fact that η is a fraction $\eta \leqslant 1$ implies that these models based on string-net IOMs will not necessarily be exactly solvable. In the Kitaev model, it turns out to be exactly solvable using an additional mapping with Majorana fermions, but this need not be a generic case. Therefore, we need to resort to other techniques in order to study the physical properties of these models. We consider here and in the next section approximate methods based on bosonic and fermionic mappings. The application of the bosonic method to our model is based on a mapping from the original spins on the blue triangles to hardcore bosons with spin [10]. With this mapping, it is possible to use the perturbative continuous unitary transformations (PCUTs) approach [83]. This is inspired by the renormalization group (RG) method based on the unitary transformation introduced by

Wegner (the similarity RG method) [84]. Originally, the PCUT method was applied to the Kitaev model [85]. As we will see below, the method paves the way to go beyond the perturbation approach presented in the preceding section which fits into a sector without any hard-core boson. The physics at other sectors is very promising and we study it here. Emergence of three families of strongly interacting anyonic fermions and invisible charges are among them, which are not present in Kitaev's model or its variants. To start with, let us set, for simplicity, $J_z = 1/4$, and consider the extreme case of $J_x = J_y = 0$. In this case, the system consists of isolated triangles. The ground states of an isolated triangle are polarized states $|\uparrow\uparrow\uparrow\rangle$ and $|\downarrow\downarrow\downarrow\rangle$ with energy $-3/4$. The excited states that appear by flipping spins are degenerate with energy $1/4$. In this limit, the spectrum of the whole system is made of equidistant levels being well suited for perturbative analysis of the spectrum: Green's function formalism as discussed in the preceding section, which may capture only the lowest orders of perturbation or another alternative approach based on the PCUT. The change from the ground state to an excited state can be interpreted as a creation of particles with energy +1. This suggests an exact mapping from the original spin degrees of freedom to quasi-particles attached to effective spins. The mapping is exact, i.e. we do not miss any degrees of freedom. Such a particle is a hard-core boson. At each site, we attach such a boson and also an effective spin-$\frac{1}{2}$. Let us choose the following bases for the new degrees of freedom:

$$|a, d\rangle = |a\rangle \otimes |d\rangle, \quad a = \Uparrow, \Downarrow, \quad d = 0, \mathrm{r}, \mathrm{g}, \mathrm{b}, \tag{39}$$

where a and d stand for states of the effective spin and quasi-particle attached to it. The Hilbert space $\mathcal{H}_C$ representing the hard-core bosons is 4D spanned by bases $\{|0\rangle, |\mathrm{r}\rangle, |\mathrm{g}\rangle, |\mathrm{b}\rangle\}$. Now the following construction relates the original spin degrees of freedom and new ones in (39):

$$\begin{aligned}
&|\Uparrow, 0\rangle \equiv |\uparrow\uparrow\uparrow\rangle, && |\Downarrow, 0\rangle \equiv |\downarrow\downarrow\downarrow\rangle,\\
&|\Uparrow, \mathrm{r}\rangle \equiv |\uparrow\downarrow\downarrow\rangle, && |\Downarrow, \mathrm{r}\rangle \equiv |\downarrow\uparrow\uparrow\rangle,\\
&|\Uparrow, \mathrm{g}\rangle \equiv |\downarrow\uparrow\downarrow\rangle, && |\Downarrow, \mathrm{g}\rangle \equiv |\uparrow\downarrow\uparrow\rangle,\\
&|\Uparrow, \mathrm{b}\rangle \equiv |\downarrow\downarrow\uparrow\rangle, && |\Downarrow, \mathrm{b}\rangle \equiv |\uparrow\uparrow\downarrow\rangle.
\end{aligned} \tag{40}$$

Within such mapping, the effective spins and hard-core bosons live at the sites of the effective hexagonal lattice Λ in figure 8(c). Recall that this lattice is produced by shrinking the triangles. At each site, we can introduce the color annihilation operator as $b_c := |0\rangle\langle c|$. The number operator n and color number operator n_c are

$$n := \sum_c n_c, \qquad n_c := b_c^\dagger b_c. \tag{41}$$

Annihilation and creation operators anti-commute on a single site, and commute at different sites; that is why they are hard-core bosons. We can also label the Pauli operators of original spins regarding their color in figure 8(b) as σ_c^w with $c = \mathrm{r}, \mathrm{g}, \mathrm{b}$. The mapping in (40) can be expressed in operator form as follows:

$$\sigma_c^z \equiv \tau^z \otimes p_c, \quad \sigma_c^\nu \equiv \tau^\nu \otimes (b_c^\dagger + b_c + s_\nu r_c), \tag{42}$$

where $\nu = x, y$, $s_x := -s_y := 1$, the symbols τ denote the Pauli operators on the effective spin and we are using the color parity operators p_c and the color switching operators r_c defined as

$$p_c := 1 - 2(n_{\bar{c}} + n_{\bar{\bar{c}}}), \qquad r_c := b_{\bar{c}}^\dagger b_{\bar{\bar{c}}} + b_{\bar{\bar{c}}}^\dagger b_{\bar{c}}. \tag{43}$$

We can now forget the original ruby lattice and work on the effective lattice in which the bosons are living at its sites. With the above identification for Pauli operators, the two-body Hamiltonian in (6) can be written in this language. Before that, let us fix a simplified notation. All spin and bosonic operators act on the sites of the effective lattice. We refer to a site by considering its position relative to a reference site: the notation $O_{,c}$ means the O applied at a site that is connected to the site of reference by a c-link. The two-body Hamiltonian then becomes

$$H = -3N/4 + Q - \sum_{\Lambda} \sum_{c \neq c'} J_{c'|c}\, T_c^{c'}, \tag{44}$$

with N being the number of sites, $Q := \sum_{\Lambda} n$ the total number of hardcore bosons, the first sum running over the N sites of the reduced lattice, the second sum running over the six combinations of different colors c, c' and

$$T_c^{c'} = u_c^{c'} + \frac{t_c^{c'} + v_c^{c'}}{2} + \frac{r_c^{c'}}{4} + \text{h.c.}, \tag{45}$$

a sum of several terms for an implicit reference site, according to the notation convention we are using. The meaning of the different terms in (45) is the following. The operator $t_c^{c'}$ is a c-boson hopping, $r_c^{c'}$ switches the color of two $\bar{c}$- or $\bar{\bar{c}}$-bosons, $u_c^{c'}$ fuses a c-boson with a $\bar{c}$-boson (or a $\bar{\bar{c}}$-boson) to give a $\bar{\bar{c}}$-boson ($\bar{c}$-boson) and $v_c^{c'}$ destroys a pair of c-bosons. The explicit expressions are

$$\begin{aligned} t_c^{c'} &:= \tau_c^{c'} b_c b_{c,c'}^{\dagger}, & r_c^{c'} &:= \tau_c^{c'} r_c r_{c,c'}, \\ u_c^{c'} &:= s_{c'|c} \tau_c^{c'} b_c r_{c,c'}, & v_c^{c'} &:= \tau_c^{c'} b_c b_{c,c'}, \end{aligned} \tag{46}$$

where we are using the notation

$$\tau_c^{c'} := \tau^{c'|c} \tau_{,c'}^{c'|c}. \tag{47}$$

We can also describe the plaquette IOM operators in figure 5 in terms of spin-boson degrees of freedom by means of the mapping in (42). For each plaquette f and color c, the plaquette operator is expressed as

$$S_f^c := \prod_{v \in f} \tau_v^{c|c'} p_{c' \star c}, \tag{48}$$

where c' is the color of the plaquette f, the product runs through its sites and $\star$ is just a convenient symmetric color operator defined by

$$c \star c := c, \qquad c \star \bar{c} := \bar{c} \star c := \bar{\bar{c}}. \tag{49}$$

The relation in (48) is just a generalization of plaquette operators in (11) to other sectors of the system. In fact taking the zero particle sector, the expressions in (11) are recovered. In the same way, the nontrivial string operators in figure 7 can be described with the above mapping as

$$S_\mu^c := \prod_{v \in \mu} \tau_v^{c|c'} p_{c \star c'}, \tag{50}$$

where μ denotes the homology class of the string. On closed surfaces, not all plaquette operators are independent. They are subject to the following constraints:

$$\prod_{f \in \Lambda} S_f^c = (-1)^{N/2}, \qquad \prod_{c=\mathbf{r},\mathbf{g},\mathbf{b}} S_f^c = (-1)^{s/2}, \tag{51}$$

where s is the number of sites of a given plaquette f. The first equation can be further divided into products over subsets of plaquettes, giving rise to other constants of motion, the so-called color charges, as

$$\prod_{f\in\Lambda_{\bar{c}}} S_f^{\bar{c}} \prod_{f\in\Lambda_{\bar{\bar{c}}}} S_f^{\bar{\bar{c}}} = \prod_{f\in\Lambda_{\bar{\bar{c}}}} S_f^{c} \prod_{f\in\Lambda_c} S_f^{\bar{c}} = \prod_{\Lambda} p_c. \tag{52}$$

In these products, the spin degrees of freedom are washed out, since they appear twice and consequently square identity. By using equation (43), the product over parity operators can be written as

$$\chi_\Lambda(c) = \prod_{\Lambda} p_c = (-1)^{Q_{\bar{c}}+Q_{\bar{\bar{c}}}}, \tag{53}$$

where $Q_c = \sum_\Lambda n_c$ is the total number of c-bosons. It is simple to check that the above equation commutes with Hamiltonian in (44). For each family of bosons, we can attach a charge. We suppose that each c-boson carries a charge as χ_c, that is, an irrep of the gauge group. In particular, the Hamiltonian preserves the following total charge:

$$\chi_\Lambda := \chi_{\mathrm{r}}^{Q_{\mathrm{r}}} \chi_{\mathrm{g}}^{Q_{\mathrm{g}}} \chi_{\mathrm{b}}^{Q_{\mathrm{b}}}. \tag{54}$$

5.1. Emerging particles: anyonic fermions

Equation (52) could already suggest that the parity of vortices is correlated to the parity of the number of bosons. In particular, creation of a c-boson changes the vorticity content of the model.

The statistics of vortices depend on their color and type as in figure 2. But what about the statistics of c-bosons? As studied in [86], the statistics of quasi-particles can be examined using the hopping terms. These hopping terms are combined so that two quasi-particles are exchanged. In addition to usual hopping terms, we also need composite hopping; that is, a c-boson hops from one c-plaquette to another, which is carried out by terms like $t_c^c = u_{\bar{\bar{c}}}^c u_{\bar{c},c}^{c\,\dagger} = u_{\bar{c}}^c u_{\bar{\bar{c}},c}^{c\,\dagger}$. Let us consider a state with two c-boson excitations located at two different sites separated from a reference site by $\bar{c}$ and $\bar{\bar{c}}$ links. An illustrative example for the case of, say, blue bosons is depicted in figure 11(a). Consider a process with the net effect of resulting in the exchange of two bosons. Each step of the process can be described by hopping terms. Upon combining hopping terms, we are left with the following phase:

$$t_c^{\bar{\bar{c}}} t_{c,c}^{c} t_c^{\bar{c}} t_{c,\bar{\bar{c}}}^{\bar{\bar{c}}} t_c^{c} t_{c,\bar{c}}^{\bar{c}} = (\tau^y \tau_{,\bar{\bar{c}}}^{y} \tau^z \tau_{,c}^{z} \tau^x \tau_{,\bar{c}}^{x})^2 = -1, \tag{55}$$

which explicitly shows that the quasi-particles made of hardcore bosons and effective spins have fermion statistics [10]. Thus, we have three families of fermions each of one color. These are high-energy fermions interacting strongly with each other due to the fusion term in the Hamiltonian. Fermions from different families have mutual semionic statistics, that is, encircling one c-fermion around a $\bar{c}$-fermion picks up a minus sign. This can also be checked by examining the hopping terms as in figure 11(a). Thus, we are dealing not only with fermions but also with anyons.

The elementary operators in (46) have a remarkable property, which is that they all commute with plaquettes and strings IOM. This naturally implies that any fermionic process leaves the vorticity content of the model unaffected. A fermionic process may correspond to hopping, splitting, fusion and annihilation driven by the terms in the Hamiltonian (45) and (46).

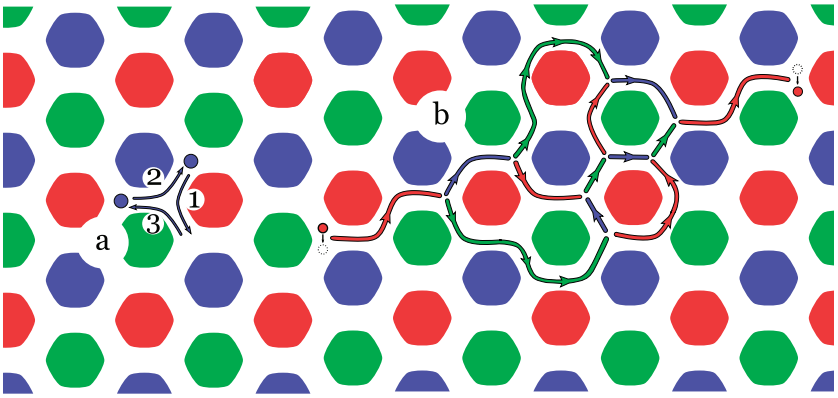

Figure 11. (a) A step by step illustration of hopping of two blue fermions with the net result of exchange of two fermions. (b) A representation of a fermionic process in which a c-fermion (here red) at the origin site is annihilated and undergoes hopping, splitting and fusion processes, and then is created at another site.

A typical fermionic process is shown in figure 11(b), with the net result of displacement of an r-fermion from a site at the origin to another site of the effective lattice. A very important feature of this process is the existence of vertexes, which are essential to high-energy fermions; that is, three fermions with different color charges can fuse into the vacuum sector. At the vertex, three different colored strings meet. Note that the colored strings shown here have nothing to do with the ones we introduced in section 3. Indeed, these are just products of some red and green links of the ruby lattice. When translated into the spin-boson language, they are responsible for the transportation of c-fermions through the lattice.

We can now think of the constraints in (52) and (53) as a correlation between the low-energy and high-energy sectors of our model. They explicitly imply that the creation of a c-fermion creates the vortices with net topological charge of $(\bar{c}, \chi_{\bar{c}})$. Alternatively, as suggested by mapping in (40), the flipping of a spin on a triangle can create or destroy the excitation; that is, a high-energy fermion can be locally transformed into low-energy ones. This amounts to attaching a topological charge from the low-energy sector to high-energy excitations. Thus a c-fermion carries a topological charge. On the other hand, an open c-string commutes with all plaquettes except some, so they create or destroy a particular charge among the charges in figure 2. It is simple to check which charge they carry at their open ends. In fact they carry $(\bar{\bar{c}}, \chi_{\bar{c}})$ charges. These latter charges have trivial mutual statistics relative to the charges carried by high-energy fermions, since they belong to different families of fermions. Thus, the charge carried by a c-string must be invisible to the high-energy fermions.

5.2. Perturbative continuous unitary transformation

The physics behind the Hamiltonian in (44) can be further explored by resorting to approximate methods. The specific form of the energy levels of our model in the isolated limit, the existence of equidistant levels, makes it suitable for perturbative continuous unitary transformations. In this method, the Hamiltonian is replaced by an effective one within unitary transformations in which the resulting effective Hamiltonian preserves the total charges, i.e. $[H^{\text{eff}}, Q] = 0$. Thus,

the analysis of the model relies on finding the effective Hamiltonian in a sector characterized by the number of charges at every order of perturbation. For our model, each sector is determined by the number of c-fermions. Each term of the effective Hamiltonian in any sector is just a suitable combination of expressions in (46) in such a way that it respects the total color charge in that sector. For now, we briefly analyze the lowest charge sectors.

In the zero-charge sector, only the effective spin degrees of freedom matter. The effective Hamiltonian is just a many-body Hamiltonian with terms that are products of plaquette operators as follows:

$$H_0^{\text{eff}} = E_0 - \sum_{\{c\}} \sum_{\{f\}} O^{c_1,\ldots,c_n}_{f_1,\ldots,f_n} S^{c_1}_{f_1} \ldots S^{c_n}_{f_n}, \tag{56}$$

where the first and second sums run over an arbitrary collection of colors and plaquettes of the effective honeycomb lattice. The coefficients O's are determined at a given order of perturbation. The product of plaquette operators is nothing but the string-net operators. Let us focus on the lowest order of perturbation, where the model represents non-interacting vortices. First, let us redefine plaquette operators as

$$B^x_f = j_x^{s/2} \prod_{v \in f} \tau^x_v, \qquad B^y_f = j_y^{s/2} \prod_{v \in f} \tau^y_v, \tag{57}$$

where $j_w := J_w/|J_w|$. At the ninth order of perturbation, the effective Hamiltonian is

$$H_0^{\text{eff}} = -\sum_{f \in \Lambda} \left(k_x B^x_f + k_y B^y_f + k_z B^x_f B^y_f \right), \tag{58}$$

with [10]

$$k_z = \tfrac{3}{8} |J_x J_y|^3 + O(J^7), \quad \frac{k_x}{|J_y|^3} = \frac{k_y}{|J_x|^3} = \frac{55\,489}{13\,824} |J_x J_y|^3. \tag{59}$$

This is exactly the many-body Hamiltonian of TCC obtained in (34) using degenerate PT with the additional advantage of knowing the coefficients exactly. Its ground state is vortex free and can be written explicitly by choosing a reference state as

$$2^{N/4-1} \prod_f \left(\frac{1 + B^x_f}{2} \right) |\Uparrow\rangle \otimes |0\rangle_b. \tag{60}$$

Other degenerate ground states can be constructed by considering the nontrivial string operators winding around the torus. Excitations above the ground state do not interact. Going to higher orders of perturbation, as the equation in (56) suggests, the ground states remain unchanged; however, the excitation spectrum changes and vortices interact with each other.

The one-quasi-particle sector can also be treated by examining the expressions in (46). The effective Hamiltonian can be written as

$$H_1^{\text{eff}} = H_0^{\text{eff}} - \sum_{\{R\}} O_R \hat{R} b^\dagger_{c,R} b_c. \tag{61}$$

What the second term describes is nothing but the annihilation of a c-fermion at a reference site and then its creation at a site connected to the reference by a string-net R, as shown in figure 11(b). Again note that this string-net is just the product of the green and red links of the original two-body Hamiltonian and in its effective form is given in terms of spin–boson degrees of freedom. The coefficients O's are determined at any order of perturbation. Note

that these coefficients are different from those in (56). In the first order, only the hopping term matters. Let us consider the sector containing a c-fermion. Up to this order, the fermion can only hop around a c-plaquette. This implies that at first order the fermion performs an orbital motion around a plaquette of its color. Note that the fermion cannot hop from a c-plaquette to other c-plaquettes at the first order, since it needs a composite process that appears at second order. This composite process is a combination of splitting and fusion processes. This is a virtual process in the sense that the splitting of a c-fermion into $\bar{c}$- and $\bar{\bar{c}}$-fermions takes the model from the one-quasi-particle sector to the two-quasi-particle sector, but the subsequent process fuses the two particles into a single one returning it back to the one-quasi-particle sector. Thus, at second order, the c-fermion can jump from one orbit to the other.

At the first order, for $J = J_x = J_y$, we obtain a $-2J$ contribution to the energy gap coming from orbital motion. Going to the second order, we get a non-flat dispersion relation. The gap, at this order, is given by $1 - 2J - J^2/2$ and thus it closes at $J \simeq 0.45$. This is just an approximate estimation, since we are omitting all fermion interactions and, perhaps more importantly, we are taking $J \simeq J_z$. However, it is to be expected that as the couplings $J_x \sim J_y$ grow in magnitude, the gap for high-energy fermions will reduce, producing a phase transition when the gap closes. Such a phase transition resembles the anyon condensations discussed in [87]–[89]. There are three topological charges invisible to the condensed anyons. This means that in the new phase there exists a residual TO related to these charges. They have semionic mutual statistics underlying the topological degeneracy in the new phase.

5.3. Fermions and gauge fields

The emerging high-energy c-fermions always appear with some nontrivial gauge fields [10, 86] and carry different representations of the gauge symmetry $\mathbf{Z}_2 \times \mathbf{Z}_2$ of the model. Before clarifying this, we can see that the plaquette degrees of freedom correspond to $\mathbf{Z}_2 \times \mathbf{Z}_2$ gauge fields. This correspondence is established via introducing the following plaquette operators:

$$\begin{aligned} B_f^{\bar{\bar{c}}} &:= j_x^{s/2}\, S_f^{\bar{c}}, \\ B_f^{\bar{c}} &:= j_y^{s/2}\, S_f^{\bar{\bar{c}}}, \\ B_f^{c} &:= (-j_x j_y)^{s/2}\, S_f^{c}. \end{aligned} \tag{62}$$

The gauge element $q_f \in \mathbf{Z}_2 \times \mathbf{Z}_2$ that can be attached to the plaquette f is determined by the following eigenvalue conditions:

$$\chi_c(q_f) = B_f^c, \tag{63}$$

which always has a solution due to

$$(B_f^c)^2 = B_f^{\mathrm{r}} B_f^{\mathrm{g}} B_f^{\mathrm{b}} = 1. \tag{64}$$

The ground state of color code Hamiltonian (58) is vortex free and corresponds to $\chi_c = 1$. The fact that, for a 2-colex with hexagonal plaquettes, the gauge fields can be related to representation of the group is immediate. One way to see this is to check the phase picked up by a c-fermion when it moves around a plaquette. Turning on a plaquette is done using a combination of hopping operators yielding the phases as $B_f^{\bar{\bar{c}}}$, $B_f^{\bar{c}}$ and B_f^{c} that are consistent with (64). However, this is not generic for all 2-colexes. For 2-colex plaquettes for which the

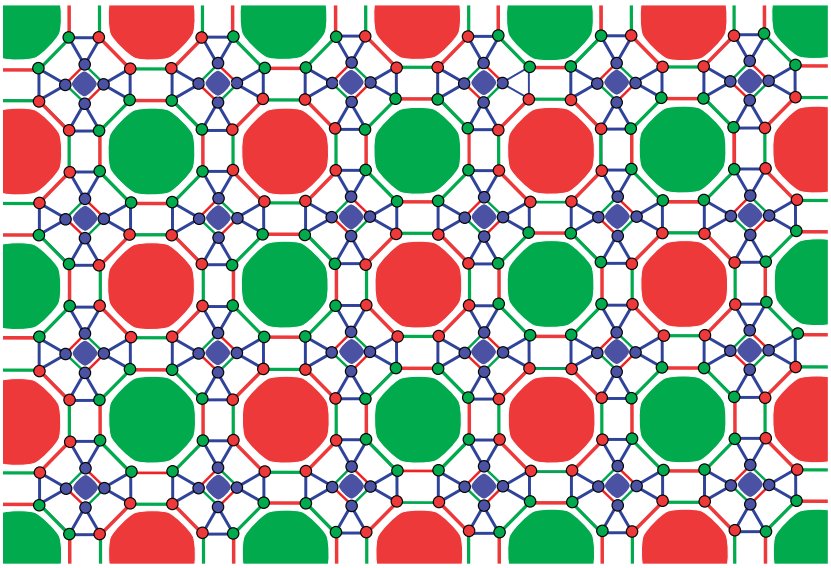

Figure 12. A piece of two-body lattice corresponding to a 2-colex composed of octagon and square plaquettes. The lattice is three-colorable as in figure 8.

number of edges is a multiple of four, we see that the ground state carries fluxes. Perhaps the most important of such lattices is the so-called 4-8-8 lattice shown in figure 12. It contains inner octagons and squares. Once degenerate PT is applied about the strong limit of the system, the effective color code Hamiltonian in terms of plaquette operators in (62) at the 12th order of perturbation is produced, as shown below:

$$H_{\text{eff}} = -\sum_{f}(k_x B_f^x + k_y B_f^y + k_z B_f^z) + \text{multiplaquette terms}, \tag{65}$$

where the sum runs over all squares and octagons. Note that at the 12th order of perturbation multi-plaquette terms that are the products of square plaquette operators also appear. It is simple to check that the coefficients k have positive sign. As we can relate the plaquettes to the representation of the gauge group, the ground state corresponds to the vortex-free sector. In fact, the ground state of all 2-colexes with plaquettes of any shape is vortex free and corresponds to $\chi_c = 1$ of the gauge group. What differentiates the ground states of 2-colex plaquettes with $4n$ (n is an integer) edges from others is the gauge fields attached to a fermion. In particular, there is a background of π-fluxes in the ground states of such lattices, and the emerging c-fermions can detect them. To make sense of the existence of such fluxes, let us consider a simple fermionic process as explained above. When a c-fermion turns on a plaquette, the combination of hopping terms yields $-B_f^{\bar{\bar{c}}}$, $-B_f^{\bar{c}}$ and $-B_f^{c}$, which clearly imply that

$$(-B_f^{\bar{\bar{c}}})(-B_f^{\bar{c}})(-B_f^{c}) = -1. \tag{66}$$

This result shows that the ground states of color code models defined on lattices with $4n$-plaquettes carry fluxes. Thus, in its representation in terms of the $\mathbf{Z}_2 \times \mathbf{Z}_2$ gauge group, the fluxes must be subtracted away.

Our derivation for ground states with 0- and π-flux can be compared with the Lieb theorem [90], which states that for a square lattice, the energy is minimized by putting π flux

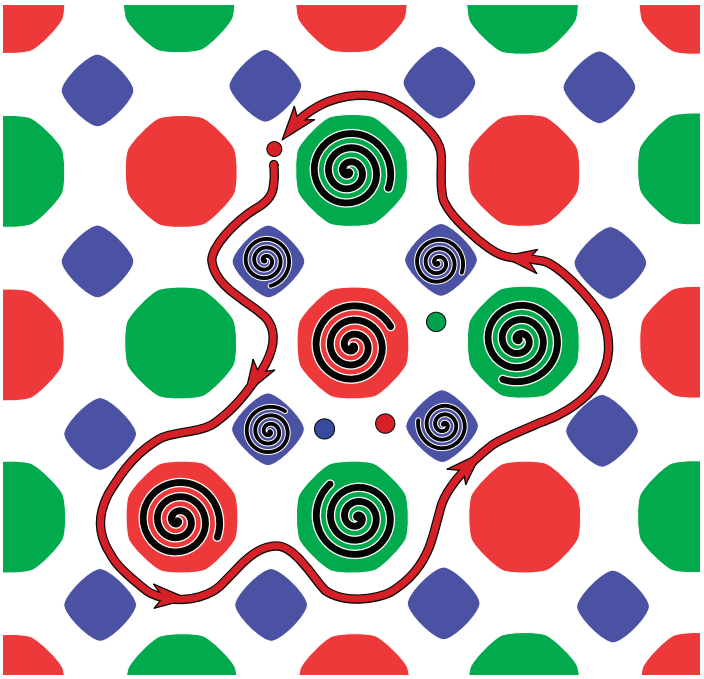

Figure 13. A c-fermion process. A red fermion goes around a region λ. The phase that it picks up depends on vortex configurations shown by spiral lines, blue and green fermions and a number of plaquettes for which the number of edges is a multiple of four.

in each square face of the lattice. The connection to our models will be seen when we consider how 2-colexes with hexagonal and 4-8-8 plaquettes can be constructed from a square lattice by removing some edges. Then the total π fluxes in a set of square faces corresponding to a 2-colex plaquette amount to the flux that it carries. It is simple to see that each hexagonal plaquette is composed of two (imaginary) square faces, and flux π in each square face then implies flux 0 in the hexagon. The same strategy holds for fluxes carried by the 4-8-8 plaquette (and, in general, for all $4n$-plaquettes). Once again we see that each plaquette of the latter 2-colexes is composed of an odd number of square faces; thus they carry flux π in their plaquettes.

Now we can give a general expression for the gauge fields seen by emerging high-energy fermions. To do so, let us consider a process in which a c-fermion is carried around a region λ, as in figure 13. The hopping process yields a phase

$$\phi_\lambda^c = \chi_c(q_\lambda)\,(-1)^{n_{\bar{c}}^\lambda + n_{\bar{\bar{c}}}^\lambda + n_4^\lambda} \tag{67}$$

where $q_\lambda = \prod_\lambda q_f$, n_c^λ denotes the number of c-fermions inside λ and n_4^λ is the number of 2-colex plaquettes inside λ for which the number of edges is a multiple of four. Thus, we can see that each family of fermions carries a different representation of the gauge group given by values of q_f inside the region. Moreover, it emphasizes that fermions with different color charges have mutual semionic statistics. Clearly, for hexagonal lattices, $n_4^\lambda = 0$, and the ground state carries no fluxes.

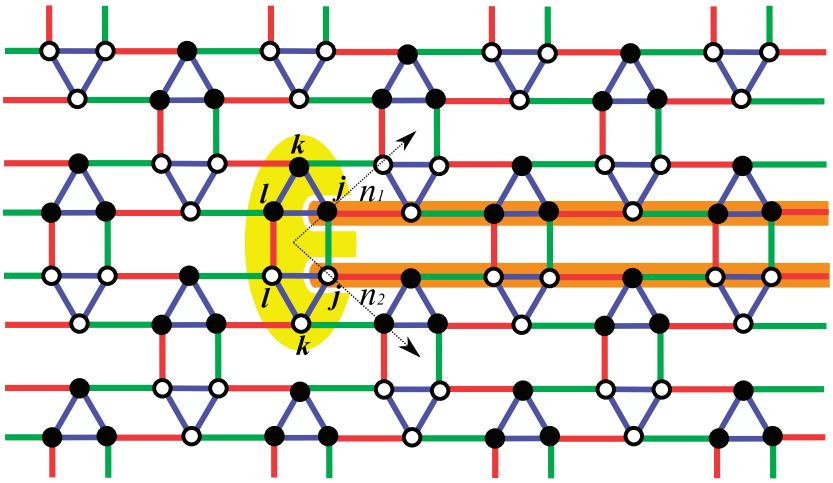

Figure 14. Brick-wall lattice that is topologically equivalent to the original lattice in figure 3. Triangles with black and white vertices are chosen such that at the logical level they correspond to a bipartite lattice. A unit cell of the lattice has been shown by the yellow region and the whole lattice can be constructed by translation vectors $\mathbf{n_1}$ and $\mathbf{n_2}$. The chains supporting the field operator F have been shown by brown ribbons.

6. Fermionic mapping

In this section, we will come back to the original Hamiltonian of (6) on the lattice in order to use another approximate method based on fermionic mappings. This Hamiltonian can be fermionized by the Jordan–Wigner transformation [73]. To do so, firstly, it is convenient to present a lattice that is topologically equivalent to the lattice of figure 3. This is a new type of 'brick-wall' lattice as shown in figure 14. The black and white sites are chosen such that, at the effective level, the lattice is a bipartite lattice, since the effective spins are located at the vertices of a hexagonal lattice representing a bipartite lattice. Note that neither the original lattice in figure 3 nor the brick-wall one in figure 14 is bipartite on its own. Also, as we will see, the fermionization of the model needs some ordering of sites in the 'brick-wall' lattice. The unit cell of the brick-wall lattice comprises two triangles as shown in figure 14 in a yellow ellipse. The translation vectors $\vec{n}_1$ and $\vec{n}_2$ connect different unit cells of the lattice.

The deformation of the original lattice into a 'brick-wall' lattice allows one to perform the 1D Jordan–Wigner transformation. The 1D structure of the lattice is considered as an array of sites on a contour as shown in figure 15. The sites on the contour can be labeled by a single index and the ordering of the sites is identified by the direction of the arrows in figure 15. The expression of the Pauli operators in terms of spinless fermions will be

$$\sigma_j^+ = a_j^\dagger \exp\left(\mathrm{i}\pi \sum_{l<j} a_l^\dagger a_l\right), \qquad \sigma_j^z = (2a_j^\dagger a_j - 1), \tag{68}$$

where spinless fermions satisfy the usual anti-commutation relations as follows:

$$\{a_i, a_j^\dagger\} = \delta_{ij}, \quad \{a_i^\dagger, a_j^\dagger\} = \{a_i, a_j\} = 0. \tag{69}$$

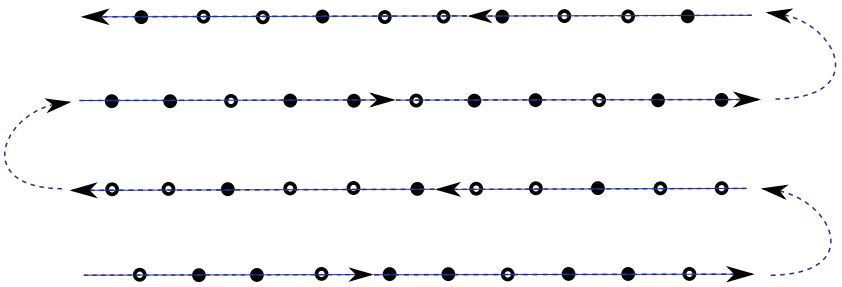

Figure 15. Ordering of sites in the brick-wall lattice of figure 14. Such ordering makes it possible to perform a 1D Jordan–Wigner transformation.

Next, we introduce Majorana fermions as follows:

$$c_j = -\mathrm{i}(a_j^\dagger - a_j), \quad d_j = a_j^\dagger + a_j \tag{70}$$

for black sites and

$$c_j = a_j^\dagger + a_j, \quad d_j = -\mathrm{i}(a_j^\dagger - a_j) \tag{71}$$

for white sites. Majorana operators are Hermitian and satisfy the following relations:

$$k_j^2 = 1, \quad k_j k_i = -k_i k_j, \quad i \neq j, \tag{72}$$

where $k = c, d$. For each unit cell, we can realize two vertical red and green links corresponding to $\sigma^x\sigma^x$ and $\sigma^y\sigma^y$ interactions. Observe that each vertex of the lattice can be specified by three indices as follows: (i) index I is introduced to specify to which unit cell the vertex belongs, (ii) b (w) denotes the black (white) vertex, (iii) l, j and k label the position of the vertex in each triangle. With this labeling of vertices, the expression of the different terms appearing in the two-body Hamiltonian in terms of Majorana fermions is listed below:

$$\begin{aligned}
&\text{Blue links:} && \sigma_j^z\sigma_k^z = \mathrm{i}\hat{U}_{jk} d_j d_k,\\
&\text{Horizontal r-links:} && \sigma_j^x\sigma_k^x = \mathrm{i} d_j d_k,\\
&\text{Horizontal g-links:} && \sigma_j^y\sigma_k^y = -\mathrm{i} d_j d_k,\\
&\text{Vertical r-links:} && \sigma_l^{(\mathrm{Iw})x}\sigma_l^{(\mathrm{Ib})x} = \mathrm{i} d_l^{(\mathrm{Iw})} d_l^{(\mathrm{Ib})} \hat{F}_{\mathrm{I}},\\
&\text{Vertical g-links:} && \sigma_j^{(\mathrm{Iw})y}\sigma_j^{(\mathrm{Ib})y} = -\mathrm{i} d_j^{(\mathrm{Iw})} d_j^{(\mathrm{Ib})} \hat{F}_{\mathrm{I}},
\end{aligned} \tag{73}$$

where $\hat{U}_{jk} = -\mathrm{i}c_j c_k$ and the operator $\hat{F}_{\mathrm{I}}$ is a non-local operator. Interestingly, this non-local term has the following expression:

$$\hat{F}_{\mathrm{I}} = \exp\left(\mathrm{i}\pi \sum_{l=j}^{k-1} a_l^\dagger a_l\right) = \prod_{l\in R} \mathrm{i} c_l d_l, \tag{74}$$

where we have used the ordering of the brick-wall lattice and R stands for a set of spins crossed by the two brown ribbons shown in figure 14.

Observe that for each unit cell, we can realize such ribbons. The non-local operator can be written as a product of some plaquette operators each corresponding to a rectangle (inner hexagon) wrapped by the ribbons. Note that an inner hexagon of the ruby lattice in figure 3 looks like a rectangle in the brick-wall lattice. Thus, the two ribbons are nothing but a combination

of rectangles as in figure 14. This plaquette operator precisely corresponds to operator S_f^C in figure 5. Let $f_1, f_2, \ldots$ stand for those rectangles (inner hexagons). Thus, we have

$$\hat{F}_{\mathrm{I}} = \prod_{l \in R} c_l d_l = S^C_{f_1} \otimes S^C_{f_2} \otimes S^C_{f_3} \cdots. \tag{75}$$

After all these transformations, we arrive at an exact fermionized Hamiltonian given by

$$H = -J_z \sum_{\text{b-link}} \mathrm{i}\hat{U}_{jk} d_j d_k - J_x \sum_{\text{r-link}} \mathrm{i} d_j d_k + J_y \sum_{\text{g-link}} \mathrm{i} d_j d_k$$
$$- J_x \sum_{\mathrm{I}} \mathrm{i} d_l^{(\mathrm{Iw})} d_l^{(\mathrm{Ib})} \hat{F}_{\mathrm{I}} + J_y \sum_{\mathrm{I}} \mathrm{i} d_j^{(\mathrm{Iw})} d_j^{(\mathrm{Ib})} \hat{F}_{\mathrm{I}}. \tag{76}$$

It is simple to check the following commutation relations:

$$[H, \hat{F}_{\mathrm{I}}] = [H, \hat{U}_{jk}] = [\hat{F}_{\mathrm{I}}, \hat{F}_{\mathrm{I}'}] = 0. \tag{77}$$

Since $\hat{F}_{\mathrm{I}}^2 = 1$, the non-local operators can be replaced by its eigenvalues $F_{\mathrm{I}} = \pm 1$. Thus, the non-local terms appearing in the Hamiltonian, which are related to the vertical links of the brick-wall lattice, can be reduced to quadratic terms. However, the first sum in (76) that is related to the triangles cannot be reduced to the quadratic term. This is because local fields $\hat{U}_{jk}$ corresponding to three links of a triangle anti-commute with each other as well as with some $\hat{F}_{\mathrm{I}}$'s. Owing to these anti-commutations, all fields cannot be fixed independently. This fact is in sharp contrast with Kitaev's model and its variants. These latter models are defined on trivalent lattices. The different fields live at spatially separated links, allowing a free fermion exact solution [72, 73]. The obtained quadratic Hamiltonian describes free Majorana fermions in a background of $\mathbf{Z}_2$ charges. Instead, the lattice of our model is four-valent, a sharp difference that prevents complete solvability and gives rise to very interesting features not present in the mentioned models. Note that the fields $\hat{U}_{jk}$ are highly interacting since on a triangle three fields go to vacuum in the sense that $\hat{U}_{jk}\hat{U}_{kl}\hat{U}_{lj} = -1$. This is the resemblance of the vertex interaction in high-energy fermions to the bosonic mapping that we have seen in section 5. However, this latter relation does not coincide with the symmetry of the model as they do not commute with each other. This will be considered next.

So far, we have considered fields that are present in the Hamiltonian. In what follows, we introduce another set of fields that have the $\mathbf{Z}_2 \times \mathbf{Z}_2$ symmetry commuting with each other and with the Hamiltonian. To this end, consider a plaquette f. As before, by a plaquette we mean an outer and an inner hexagon with six triangles between them. Let V_f and V_h stand for sets of vertices of the plaquette and inner hexagon, respectively. It is natural that $V_h \subset V_f$. To each plaquette, we attach the following three fields:

$$\phi_f^1 = \prod_{j \in V_f} c_j, \quad \phi_f^2 = \prod_{j \in f \setminus h} c_j \prod_{v \in V_h} d_j, \quad \phi_f^3 = \prod_{j \in V_h} c_j d_j, \tag{78}$$

where by $f \setminus h$ we simply mean $V_f - V_h$. Each ϕ_f squares identity. They commute with each other and with the Hamiltonian and $\hat{F}_{\mathrm{I}}$:

$$\left[\phi_f^k, \phi_{f'}^{k'}\right] = \left[\phi_f^k, \hat{F}_{\mathrm{I}}\right] = \left[H, \phi_f^k\right] = 0. \tag{79}$$

Also, the fields ϕ_f are responsible for the $\mathbf{Z}_2 \times \mathbf{Z}_2$ gauge symmetry since $\phi_f^1 \otimes \phi_f^2 \otimes \phi_f^3 = -1$. The above fields are related to the plaquette operators. Using the transformations we have

introduced in (73), we can fermionize the conserved plaquette operators obtained in figure 5. They are associated with the above constants of motion as follows:

$$S_f^A = \phi_f^1 \hat{F}_{\mathrm{I}}, \quad S_f^B = \phi_f^2 \hat{F}_{\mathrm{I}}, \quad S_f^C = \phi_f^3. \tag{80}$$

Although the above gauge fields make it possible to divide the Hilbert space into sectors which are eigenspaces of gauge fields (or eigenspaces of plaquette operators), they do not allow us to reduce the Hamiltonian in (76) into a quadratic form. The $\hat{F}_{\mathrm{I}}$'s can be fixed as they commute with the Hamiltonian. But we are not able to reduce the four-body interaction terms in the Hamiltonian into quadratic form. In fact, the anti-commutation of $\hat{U}_{jk}$'s on a blue triangle prevents them from being fixed consistently with gauge fixing.

7. Conclusions

We have introduced a two-body spin-$\frac{1}{2}$ model in a ruby lattice (see figure 3). The model exhibits an exact topological degeneracy in all coupling regimes. The connection to the TCCs can be discussed on the non-perturbative level and confirmed by perturbative methods. In the former case, on the ruby lattice we realized plaquette operators with local $\mathbf{Z}_2 \times \mathbf{Z}_2$ symmetry of the color codes. All plaquette operators commute with the Hamiltonian and they correspond to IOM. The plaquettes can be extended to more complex objects that can be considered as string-nets: nontrivial strings with branching points. The nontrivial strings corresponding to the various homology classes of the manifold determine the exact degeneracy of the model. For the case of periodic boundary conditions, i.e. on a torus, and for each non-contractible cycle of the torus, we can identify three nontrivial closed strings. Once each of them is colored, the plaquettes of the lattice can be correspondingly colored as in figure 8. For each homology class, they are related to each other by the gauge symmetry of the model. The crucial property of these strings is that they commute with the Hamiltonian but not always with each other. This is independent of the regimes of coupling constants of the model. Being anti-commuting closed nontrivial strings, the model has exact topological degeneracy. To clarify this observation, we use PT to investigate a regime of coupling corresponding to a strong coupling limit (triangular limit). In this limit, the TCC will be the effective description of the model. The effective representation of the closed loop operators determines the terms appearing in the effective Hamiltonian at different orders.

Unlike Kitaev's model or any of its variants, our model is not integrable in terms of mapping to Majorana fermions, to the best of our knowledge. This model is a four-valent lattice and gauge fields do not always commute with each other. However, we have emphasized in section 3 that the existence of exact IOM at a non-perturbative level is far more enriching than demanding exact solvability of a model. In fact, if the number of IOM is large enough, the model can turn out to be solvable. Thus, fixing plaquette operators cannot give rise to fixing all gauge fields.

The description of our model in terms of hard core bosons yields very fruitful and interesting physics of the model. Using a bosonic mapping, it is possible to discuss the emergence of strongly interacting anyonic fermions. They form three classes each of one color. Fermions from different classes have mutual semionic statistics. A very intriguing feature of these fermions is related to the topological color charges they carry. They carry charges from a particular family of low-energy fermions. Thus the charges created by open strings are invisible to high-energy fermions. Moreover, there are some experimental proposals to realize hard-core

bosons with optical lattices [91] and it would be a nice challenge to implement a Hamiltonian like (44) and (45).

We have shown that this new model exhibits enough novel, interesting and relevant properties to justify further research on it. Some of these possible lines of study are as follows: we have only studied a particular phase of the system, although we can study non-perturbative effects as well. The fact that all phases show a topological degeneracy anticipates a rich phase diagram. In this regard, one may explicitly break the color symmetry that the model exhibits and still keep the features that we have discussed. It would be particularly interesting to check whether any of the phases displays non-Abelian anyons. The model has many IOMs, although not enough to make it exactly solvable. This becomes another appealing feature of the model since other methods of study, such as numerical simulations and experimental realizations, will help us to gain a complete understanding of all its phases.

Acknowledgments

We acknowledge financial support from a PFI grant of EJ-GV, DGS grants under contract FIS2006-10061 and the ESF INSTANS 2005-10.

Appendix. Two-body Hamiltonian for color codes using cluster states

A TCC can be constructed from a graph state defined on a bipartite lattice by means of a set of measurements on certain subsystems. This bipartite lattice is shown in figure A.1(a), where the black vertices correspond to plaquettes and the white vertices correspond to the vertices of a 2-colex. To this graph we can attach a set of stabilizers, as shown below:

$$K_\alpha = X_\alpha \prod_{\prec\alpha,\beta\succ} Z_\beta, \tag{A.1}$$

where α and β stand for vertices of the graph and the product runs over all vertices that are connected to α by black links. Let us set $V = \mathfrak{U}_1 \cup \mathfrak{U}_2$, where $\mathfrak{U}_1$ and $\mathfrak{U}_2$ stand for the set of white and black vertices of the bipartite graph in figure A.1(a). Note that white and black vertices correspond to the vertices and plaquettes of the 2-colex. This bipartite graph is exactly what we need to construct color codes. To this end, we first impose a unitary transformation on the sublattices that allows us to have a more symmetric form of the stabilizer operators, that is,

$$\begin{aligned} &\forall\ v \in \mathfrak{U}_1, \quad K_v = X_{N(v)}, \\ &\forall\ f \in \mathfrak{U}_2, \quad K_f = Z_{N(f)}, \end{aligned} \tag{A.2}$$

where $N(v)$ denotes the site v and its neighbors, and the same goes for $N(f)$. The corresponding cluster state denoted by $|G\rangle$ will be the common eigenvector of the above stabilizer operators. Thus, we have

$$\begin{aligned} &\forall\ v \in \mathfrak{U}_1, \quad X_{N(v)}|G\rangle = |G\rangle, \\ &\forall\ f \in \mathfrak{U}_2, \quad Z_{N(f)}|G\rangle = |G\rangle. \end{aligned} \tag{A.3}$$

Finally, a graph state can be related to a color code within a set of measurements in the Z basis on all qubits corresponding to the set $\mathfrak{U}_2$.

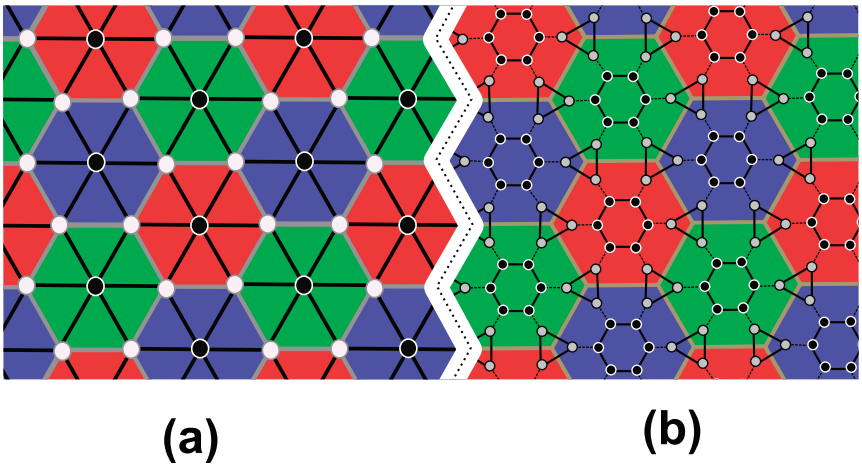

Figure A.1. (a) The graph needed for obtaining color codes from graph states. The graph is bipartite. Black and white vertices correspond to the plaquettes and vertices of a 2-colex. Black solid links are edges of the graph. (b) The corresponding graph state can be approximated as a low-energy description of a lattice with two-body Hamiltonian. The lattice is obtained from the graph by replacing its vertices with some hexagons and triangles. The interactions $\sigma^z\sigma^z$ and $\sigma^x\sigma^z$ are associated with the solid and dashed links, respectively.

We suppose that there is a 2D lattice of physical qubits that is governed by a two-body Hamiltonian. Physical qubits of the lattice are projected to *logical* qubits. The point is that this projection is achieved by going to some order in PT. We think of the vertices of the graph in figure A.1(a) as logical qubits. The lattice with two-body interaction is shown in figure A.1(b), where the number of physical qubits corresponding to the vertices of the graph equals the number of links crossing the vertex. The new resulting lattice consists of *triangles* and *hexagons* and physical qubits live on their vertices. Triangles and hexagons are in one-to-one correspondence with the white and black vertices ($\mathfrak{U}_1$ and $\mathfrak{U}_2$) of the graph in figure A.1(b), respectively. Note that each triangle is linked with three neighboring hexagons and each hexagon is linked with six neighboring triangles.

The low-lying spectrum of a well-constructed two-body Hamiltonian defined on the lattice composed of hexagons and triangles may describe a cluster state. To this end, we need the following projection from the physical qubits to the logical ones:

$$P_v = |\Uparrow_v\rangle\langle\uparrow\uparrow\uparrow| + |\Downarrow_v\rangle\langle\downarrow\downarrow\downarrow|, \qquad P_f = |\Uparrow_f\rangle\langle\uparrow\uparrow\uparrow\uparrow\uparrow\uparrow| + |\Downarrow_f\rangle\langle\downarrow\downarrow\downarrow\downarrow\downarrow\downarrow|, \tag{A.4}$$

where $|\Uparrow_L\rangle$ and $|\Downarrow_L\rangle$ with $L = v$ and f stand for the two states of the logical qubits obtained within the above projections or, alternatively, they are states of logical qubits of the graph in figure A.1(a). We set the following Hamiltonian:

$$H = H_0 + \lambda V, \tag{A.5}$$

where H_0 is the unperturbed Hamiltonian that can be treated exactly and λ is a small quantity that allows us to treat the term λV perturbatively. We refer to each triangle (hexagon) and its vertices by a site index v (f) and indices i and j, respectively. The unperturbed part of the

Hamiltonian included in H_0 is as follows:

$$H_0 = -\sum_L \sum_{\langle i,j\rangle} \sigma^z_{L,i}\sigma^z_{L,j}, \tag{A.6}$$

where the first sum runs over all triangles and hexagons (sites) and $\langle i, j\rangle$ stand for the nearest-neighbor qubits around the corresponding triangle or hexagon connected by the solid lines as in figure A.1(b). The interaction between qubits of triangles and qubits of hexagons is included in V:

$$V = -\sum_{\langle vi,fj\rangle} (\sigma^x_{v,i}\sigma^z_{f,j} + \sigma^z_{v,i}\sigma^x_{f,j}), \tag{A.7}$$

where $\langle vi, fj\rangle$ denotes two neighboring qubits that are connected by the dashed line. The unperturbed Hamiltonian H_0 can easily be diagonalized for triangles and hexagons. Ground state vectors of a triangle or hexagon form a 2D space spanned by the following polarized eigenvectors:

$$\text{triangle: } |\Uparrow_v\rangle \equiv |\uparrow\uparrow\uparrow\rangle, \quad |\Downarrow_v\rangle \equiv |\downarrow\downarrow\downarrow\rangle \tag{A.8}$$

and

$$\text{hexagon: } |\Uparrow_f\rangle \equiv |\uparrow\uparrow\uparrow\uparrow\uparrow\uparrow\rangle, \quad |\Downarrow_f\rangle \equiv |\downarrow\downarrow\downarrow\downarrow\downarrow\downarrow\rangle. \tag{A.9}$$

Let N_v and N_f be the number of triangles and hexagons, respectively. Imposing periodic boundary conditions, the total number of triangles and hexagons will be: $N = N_v + N_f = 3N_f$. Thus, the dimension of the ground space of the unperturbed Hamiltonian H_0 (or ground state degeneracy) becomes: $g_0 = 2^{N_v}2^{N_f} = 2^N$, and the ground state energy is: $E_0^{(0)} = N_f(-6) + N_v(-3) = -4N$ in terms of the energy scale of the problem. The first excited state is produced by exciting one of the triangles or hexagons and has energy: $E_1^{(0)} = N_f(-6) + N_v(-3) + 4 = -4(N-1)$ with degeneracy $g_1 = 14N2^N$. The second excited state has energy $E_1^{(0)} = N_f(-6) + N_v(-3) + 8 = -4(N-2)$ with degeneracy: $g_2 = 4(N + 5N^2)2^{N-1}$, and so on and so forth.

Using degenerate PT as in section 4.2, the effect of perturbation V on the ground state subspace can be investigated, and it can be seen whether it breaks the degeneracy. It is clearly seen that the first-order perturbation does not have anything to do with the ground state subspace. The second order gives rise to a trivial effect as a shift in energy, since each operator related to dashed links appears twice. The third-order PT, however, gives rise to a nontrivial effect. It causes a partial lift of the ground state degeneracy, but not a complete one. The initial degeneracy 2^N gets reduced down to 2^{N_f}. This nontrivial effect arises from the product of three dashed links crossing a typical triangle, namely the ground state vectors are grouped into the 2^{N_v} states, each containing 2^{N_f} vectors. The product of three (six) σ^x operators around a triangle (hexagon) is equivalent to an X operator acting on the logical qubit, which is projected down from the three (six) qubits of the triangle (hexagon), since

$$X_L = |\Uparrow_L\rangle\langle\Downarrow_L| + |\Downarrow_L\rangle\langle\Uparrow_L|. \tag{A.10}$$

Also the action of a σ^z on one qubit of a triangle or hexagon is equivalent to an Z operator acting on the related logical qubit, since

$$Z_L = P_L\sigma^z P_L^\dagger = |\Uparrow_L\rangle\langle\Uparrow_L| - |\Downarrow_L\rangle\langle\Downarrow_L|. \tag{A.11}$$

Now we can proceed to calculate the third-order perturbation:

$$H^{(3)}_{\text{eff}} = -\frac{3!}{(E_0^{(0)} - E_1^{(0)})^2}\sum_v K_v = -\delta\sum_v K_v, \tag{A.12}$$

where

$$K_v = X_v \prod_f Z_f, \tag{A.13}$$

the product runs over three black vertices linked to the v and $\delta = \frac{3}{8}$. The operator K_v is a stabilizer for the logical qubits that are projected down from the triangles. Since $K_v^2 = 1$, the ground states correspond to the values of $k_v = +1$. We skip the fourth and the fifth order of perturbation because they have trivial effects.

Like in third-order perturbation, we are faced with a nontrivial term in the sixth-order PT. We will see that by considering this order, the ground state degeneracy is lifted completely. This nontrivial effect arises from the product of terms in the perturbation λV corresponding to the links around a hexagon. Finally, for the sixth-order perturbation, we have

$$H_{\text{eff}}^{(6)} = -\gamma \sum_f K_f, \tag{A.14}$$

where

$$K_f = X_f \prod_v Z_v, \tag{A.15}$$

and the product runs over six white vertices linked to the hexagon f. The coefficient γ has positive sign and its precise value is unimportant. We would like to emphasize that at sixth order in PT, some other terms appear, which are products of two distinct K_v. However, we skip them as they all commute. Equations (A.13) and (A.15) provide all that we need to adopt the cluster state in (A.3) as the ground state of the low energy effective theory of the Hamiltonian in (A.5), which up to the sixth order of perturbation can be written as follows:

$$H_{\text{eff}} = \text{constant} - \delta \sum_v K_v - \gamma \sum_f K_f. \tag{A.16}$$

We see that the above effective Hamiltonian is completely different from that in (34). The latter equation gives rise directly to the TCC as its ground state, but the ground state (cluster state) of the former needs further local measurements to encode the desired color code.

References

[1] Bombin H and Martin-Delgado M A 2006 Topological quantum distillation *Phys. Rev. Lett.* **97** 180501 (arXiv:quant-ph/0605138)

[2] Bombin H and Martin-Delgado M A 2007 Topological computation without braiding *Phys. Rev. Lett.* **98** 160502 (arXiv:quant-ph/0610024)

[3] Bombin H and Martin-Delgado M A 2007 Exact topological quantum order in $D = 3$ and beyond: branyons and brane-net condensates *Phys. Rev.* B **75** 075103 (arXiv:cond-mat/0607736)

[4] Briegel H J and Raussendorf R 2001 *Phys. Rev. Lett.* **86** 910

[5] Raussendorf R and Briegel H J 2001 *Phys. Rev. Lett.* **86** 5188
Raussendorf R and Briegel H J 2002 *Quantum Inf. Comput.* **2** 443

[6] Raussendorf R, Browne D E and Briegel H J 2003 *Phys. Rev.* A **68** 022312

[7] Bombin H and Martin-Delgado M A 2008 Statistical mechanical models and topological color codes *Phys. Rev.* A **77** 042322 (arXiv:0711.0468)

[8] Bartlett S D and Rudolph T 2006 *Phys. Rev.* A **74** 040302

[9] Van den Nest M, Luttmer K, Dür W and Briegel H J 2008 *Phys. Rev.* A **77** 012301

[10] Bombin H, Kargarian M and Martin-Delgado M A 2009 Interacting anyonic fermions in a two-body 'color code' model *Phys. Rev.* B **80** 075111 (arXiv:0811.0911)
[11] Nielsen M and Chuang I 2000 *Quantum Computation and Quantum Information* (Cambridge, UK: Cambridge University Press)
[12] Galindo A and Martin-Delgado M A 2002 Information and computation: classical and quantum aspects *Rev. Mod. Phys.* **74** 347 (arXiv:quant-ph/0112105)
[13] Levy J E, Ganti A, Phillips C A, Hamlet B R, Landahl A J, Gurrieri T M, Carr R D and Carroll M S 2009 The impact of classical electronics constraints on a solid-state logical qubit memory (arXiv:0904.0003)
[14] Micheli A, Brennen G K and Zoller P 2006 A toolbox for lattice spin models with polar molecules *Nat. Phys.* **2** 341 (arXiv:quant-ph/0512222)
[15] Jiang L, Brennen G K, Gorshkov A V, Hammerer K, Hafezi M, Demler E, Lukin M D and Zoller P 2008 Anyonic interferometry and protected memories in atomic spin lattices *Nat. Phys.* **4** 482 (arXiv:0711.1365)
[16] Müller M, Liang L, Lesanovsky I and Zoller P 2008 Trapped Rydberg ions: from spin chains to fast quantum gates *New J. Phys.* **10** 093009 (arXiv:0709.2849)
[17] Duan L-M, Demler E and Lukin M D 2003 Controlling spin exchange interactions of ultracold atoms in optical lattices *Phys. Rev. Lett.* **91** 090402 (arXiv:cond-mat/0210564)
[18] Garcia-Ripoll J J, Martin-Delgado M A and Cirac J I 2004 Implementation of spin Hamiltonians in optical lattices *Phys. Rev. Lett.* **93** 250405
[19] Hartmann M J, Brandao F G S L and Plenio M B 2006 Strongly interacting polaritons in coupled arrays of cavities *Nat. Phys.* **2** 849 (arXiv:quant-ph/0606097)
[20] Lewenstein M, Sanpera A, Ahufinger V, Damski B, Sen A and Sen U 2007 Ultracold atomic gases in optical lattices: mimicking condensed matter physics and beyond *Adv. Phys.* **56** 243
[21] Du J, Zhu J, Shi M, Peng X and Suter D 2007 Experimental observation of a topological phase in the maximally entangled state of a pair of qubits *Phys. Rev.* A **76** 042121 (arXiv:0705.3566)
[22] Albuquerque A F, Katzgraber H G, Troyer M and Blatter G 2008 Engineering exotic phases for topologically protected quantum computation by emulating quantum dimer models *Phys. Rev.* B **78** 014503
[23] Brennen G K, Aguado M and Cirac J I 2009 Simulations of quantum double models arXiv:0901.1345
[24] Wilczek F 1982 Quantum mechanics of fractional-spin particles *Phys. Rev. Lett.* **49** 957
[25] Leinaas J M and Myrheim J 1977 On the theory of identical particles *Nuovo Cimento* B **37** 1
[26] Moore G and Read N 1991 Nonabelions in the fractional quantum Hall effect *Nucl. Phys.* B **360** 362
[27] Wen X G 2004 *Quantum Field Theory of Many-body Systems: From the Origin of Sound to an Origin of Light and Electrons* (Oxford: Oxford University Press)
[28] Wen X G 1995 Topological orders and edge excitations in fractional quantum Hall states *Adv. Phys.* **44** 405
[29] Bombin H and Martin-Delgado M A 2008 Interferometry-free protocol for demonstrating topological order *Phys. Rev.* B **78** 165128 (arXiv:0705.0007)
[30] Gottesman D 1996 Class of quantum error-correcting codes saturating the quantum Hamming bound *Phys. Rev.* A **54** 1862
[31] Evans Z W E and Stephens A M 2009 Optimal decoding in fault-tolerant concatenated quantum error correction arXiv:0902.4506
[32] Evans Z W E and Stephens A M 2009 Accuracy threshold for concatenated error detection in one dimension arXiv:0902.2658
[33] Kitaev A Yu 2003 Fault-tolerant quantum computation by anyons *Ann. Phys.* **303** 2 (arXiv:quant-ph/9707021)
[34] Bombin H and Martin-Delgado M A 2007 Homological error correction: classical and quantum codes *J. Math. Phys.* **48** 052105 (arXiv:quant-ph/0605094)
[35] Bombin H and Martin-Delgado M A 2006 Topological quantum error correction with optimal encoding rate *Phys. Rev.* A **73** 062303 (arXiv:quant-ph/0602063)
[36] Albuquerque C D, Palazzo R and Silva E B 2009 Topological quantum codes on compact surfaces with genus $g \geqslant 2$ *J. Math. Phys.* **50** 023513
[37] Bullock S and Brennen G K 2007 Qudit surface codes and gauge theory with finite cyclic groups *J. Phys. A: Math. Theor.* **40** 3481

[38] Bombin H and Martin-Delgado M A 2007 Optimal resources for topological 2D stabilizer codes: comparative study *Phys. Rev.* A **76** 012305 (arXiv:quant-ph/0703272)
[39] Planat M and Kibler M R 2008 Unitary reflection groups for quantum fault tolerance arXiv:0807.3650
[40] Georgiev L S 2008 Computational equivalence of the two inequivalent spinor representations of the braid group in the topological quantum computer based on Ising anyons arXiv:0812.2337
[41] Hu D, Tang W, Zhao M, Chen Q, Yu S and Oh C H 2008 Graphical nonbinary quantum error-correcting codes *Phys. Rev.* A **78** 012306 (arXiv:0801.0831)
[42] Georgiev L S 2008 Towards a universal set of topologically protected gates for quantum computation with Pfaffian qubits *Nucl. Phys.* B **789** 552
[43] Bombin H and Martin-Delgado M A 2009 Quantum measurements and gates by code deformation *J. Phys. A: Math. Theor.* **42** 095302 (arXiv:0704.2540)
[44] Raussendorf R, Harrington J and Goyal K 2007 Topological fault-tolerance in cluster state quantum computation *New J. Phys.* **9** 199 (arXiv:quant-ph/0703143)
[45] Raussendorf R and Harrington J 2007 Fault-tolerant quantum computation with high threshold in two dimensions *Phys. Rev. Lett.* **98** 190504 (arXiv:quant-ph/0610082)
[46] DiVincenzo D P 2009 Fault tolerant architectures for superconducting qubits arXiv:0905.4839
[47] Dennis E, Kitaev A, Landahl A and Preskill J 2002 Topological quantum memory *J. Math. Phys.* **43** 4452–505
[48] Katzgraber H G, Bombin H and Martin-Delgado M A 2009 Error threshold for color codes and random 3-body Ising models *Phys. Rev. Lett.* **103** 090501 (arXiv:0902.4845)
[49] Ohzeki M 2009 Threshold of topological color code arXiv:0903.2102
[50] Gao W-B *et al* 2009 Experimental demonstration of topological error correction arXiv:0905.1542v2
[51] Alicki R, Fannes M and Horodecki M 2007 A statistical mechanics view on Kitaev's proposal for quantum memories *J. Phys. A: Math. Theor.* **40** 6451–67
[52] Alicki R, Fannes M and Horodecki M 2008 On thermalization in Kitaev's 2D model arXiv:0810.4584
[53] Alicki R, Horodecki M, Horodecki P and Horodecki R 2008 On thermal stability of topological qubit in Kitaev's 4D model arXiv:0811.0033
[54] Iblisdir S, Perez-Garcia D, Aguado M and Pachos J 2008 Thermal states of anyonic systems arXiv:0812.4975
[55] Iblisdir S, Perez-Garcia D, Aguado M and Pachos J 2008 Scaling law for topologically ordered systems at finite temperature arXiv:0806.1853
[56] Bravyi S and Terhal B 2008 A no-go theorem for a two-dimensional self-correcting quantum memory based on stabilizer codes arXiv:0810.1983
[57] Kargarian M 2009 Finite temperature topological order in 2D topological color codes *Phys. Rev.* A **80** 012321 (arXiv:0904.4492)
[58] Kargarian M 2008 Entanglement properties of topological color codes *Phys. Rev.* A **78** 062312 (arXiv:0809.4276)
[59] Tu H-H, Zhang G-M, Xiang T, Liu Z-X and Ng T-K 2009 Topologically distinct classes of valence bond solid states with their parent Hamiltonians arXiv:0904.0550
[60] Pakman A and Parnachev A 2008 Topological entanglement entropy and holography *J. High Energy Phys.* JHEP07(2008)097 (arXiv:0805.1891)
[61] Rico E and Briegel H J 2008 2D multipartite valence bond states in quantum anti-ferromagnets *Ann. Phys.* **323** 2115 (arXiv:0710.2349)
[62] Eisert J, Cramer M and Plenio M B 2010 Area laws for the entanglement entropy *Rev. Mod. Phys.* **82** 277
[63] Dür W and Briegel H J 2007 Entanglement purification and quantum error correction *Rep. Prog. Phys.* **70** 1381 (arXiv:0705.4165)
[64] Karimipour V 2009 A complete characterization of the spectrum of the Kitaev model on spin ladders arXiv:0904.3554
[65] Van den Nest M, Dür W and Briegel H J 2007 Classical spin models and the quantum-stabilizer formalism *Phys. Rev. Lett.* **98** 117207 (arXiv:quant-ph/0610157)
[66] Bravyi S and Raussendorf R 2006 Measurement-based quantum computation with the toric code states *Phys. Rev.* A **76** 022304 (arXiv:quant-ph/0610162)

[67] Van den Nest M, Dür W and Briegel H J 2007 Completeness of the classical 2D Ising model and universal quantum computation arXiv:0708.2275
[68] Van den Nest M, Dür W, Raussendorf R and Briegel H J 2008 Quantum algorithms for spin models and simulable gate sets for quantum computation arXiv:0805.1214
[69] Hübener R, Van den Nest M, Dür W and Briegel H J 2008 Classical spin systems and the quantum stabilizer formalism: general mappings and applications arXiv:0812.2127
[70] De las Cuevas G, Dür W, Van den Nest M and Briegel H J 2008 Completeness of classical spin models and universal quantum computation arXiv:0812.2368
[71] De las Cuevas G, Dür W, Briegel H J and Martin-Delgado M A 2009 Unifying all classical spin models in a lattice gauge theory *Phys. Rev. Lett.* **102** 230502 (arXiv:0812.3583)
[72] Kitaev A Yu 2006 Anyons in an exactly solved model and beyond *Ann. Phys.* **321** 2 (arXiv:cond-mat/0506438v3)
[73] Feng X-Y, Zhang G-M and Xiang T 2007 Topological characterization of quantum phase transitions in a spin-1/2 model *Phys. Rev. Lett.* **98** 087204 (arXiv:cond-mat/0610626)
[74] Yao H and Kivelson S A 2007 Exact chiral spin liquid with non-abelian anyons *Phys. Rev. Lett.* **99** 247203 (arXiv:0708.0040)
[75] Baskaran G, Mandal S and Shankar R 2007 Exact results for spin dynamics and fractionalization in the Kitaev model *Phys. Rev. Lett.* **98** 247201
[76] Yang S, Zhou D L and Sun C P 2007 Mosaic spin models with topological order *Phys. Rev.* B **76** 180404 (arXiv:0708.0676)
[77] Si T and Yu Y 2008 Anyonic loops in three-dimensional spin liquid and chiral spin liquid *Nucl. Phys.* B **803** 428 (arXiv:0712.4231)
[78] Mandal S and Surendran N 2009 Exactly solvable Kitaev model in three dimensions *Phys. Rev.* B **79** 024426
[79] Levin M and Wen X-G 2005 String-net condensation: a physical mechanism for topological phases *Phys. Rev.* B **71** 045110
[80] Oshikawa M and Senthil T 2006 Fractionalization, topological order and quasiparticle statistics *Phys. Rev. Lett.* **96** 060601
[81] Bergman D L, Shindou R, Fiete G A and Balents L 2007 Degenerate perturbation theory of quantum fluctuations in a pyrochlore antiferromagnet *Phys. Rev.* B **75** 094403
[82] Kells G, Bolukbasi A T, Lahtinen V, Slingerland J K, Pachos J K and Vala J 2008 Topological degeneracy and vortex manipulation in Kitaev's honeycomb model *Phys. Rev. Lett.* **101** 240404
[83] Knetter C and Uhrig G 2000 Perturbation theory by flow equations: dimerized and frustrated $S = 1/2$ chain *Eur. Phys. J.* B **13** 209
[84] Wegner F 1994 Flow-equations for Hamiltonians *Ann. Phys.* **506** 77
[85] Vidal J, Schmidt K P and Dusuel S 2008 Perturbative approach to an exactly solved problem: Kitaev honeycomb model *Phys. Rev.* B **78** 245121 (arXiv:0809.1553)
[86] Levin M and Wen X-G 2003 Fermions, strings and gauge fields in lattice spin models *Phys. Rev.* B **67** 245316
[87] Bombin H and Martin-Delgado M A 2008 Family of non-Abelian Kitaev models on a lattice: topological condensation and confinement *Phys. Rev.* B **78** 115421
[88] Bombin H and Martin-Delgado M A 2008 Nested topological order arXiv:0803.4299
[89] Bais F A and Slingerland J K 2009 Condensate-induced transitions between topologically ordered phases *Phys. Rev.* B **79** 045316 (arXiv:0808.0627)
[90] Lieb E H 2009 The flux phase of the half-filled band *Phys. Rev. Lett.* **73** 2158
[91] Capogrosso-Sansone B, Trefzger C, Lewenstein M, Zoller P and Pupillo G 2009 Quantum phases of cold polar molecules in 2D optical lattices arXiv:0906.2009